CHAPTER FOUR

Membrane Electrostatics—A Statistical Mechanical Approach to the Functional Density Theory of Electric Double Layer

Klemen Bohinc,[1,2] Tomaž Slivnik,[1] Aleš Iglič,[1] *and* Veronika Kralj-Iglič[3,*]

Contents

Abstract

We describe physical properties of the electric double layer composed of a charged surface in contact with a solution of counter-ions and coions representing nanoparticles. The electrostatic free energy of the electric double layer is derived using a statistical mechanical approach. The consistently related expressions for the equilibrium ion and solvent distribution functions and the differential equation for the electric potential are derived by minimization of the elctrostatic free energy of the system. The finite size of nanoparticles constituting the solution is taken into account by means of the excluded

* Corresponding author. Tel.: +386 1 5437620; Fax: +386 1 4768 850;
E-mail address: veronika.kralj-iglic@fe.uni-lj.si.

[1] Laboratory of Physics, Faculty of Electrical Engineering, University of Ljubljana, Ljubljana, Slovenia
[2] Faculty of Health Studies, University of Ljubljana, Ljubljana, Slovenia
[3] Laboratory of Clinical Biophysics, Faculty of Medicine, University of Ljubljana, Ljubljana, Slovenia

Advances in Planar Lipid Bilayers and Liposomes, Volume 8
ISSN 1554-4516, DOI: 10.1016/S1554-4516(08)00204-4

volume within the lattice model. Different geometries of the electric double layer are considered. We found that an increased size of charged nanoparticles (ions) reduces the number of counter-ions near the charged surface, leading to an enhancement of the electrostatic surface potential. The linearized Poisson–Boltzmann theory and the influence of the finite size of ions (nanoparticles) on the thickness of the electric double layer are described.

Also the intra-ionic correlations within charged nanoparticles, which have spatially distributed (quadrupolar or dipolar) electric charge, are considered. The interaction between two charged surfaces in the solution composed of charged quadrupolar (divalent) or dipolar rod-like nanoparticles is calculated. It is shown that for large enough dimensions of charged quadrupolar (divalent) nanoparticles and for large enough surface charge densities of the charged surfaces, two equally charged surfaces experience attractive force owing to spatially distributed charge within the nanoparticles. Also, it is shown that in the vicinity of the charged surface (wall), large rod-like quadrupolar or dipolar nanoparticles orient in the electric field within the electric double layer. Close to the charged surfaces the orientation of the rod-like quadrupolar or the dipolar nanoparticles is hindered because of steric restrictions (hard wall).

1. Introduction

Biopolymers (DNA, polyelectrolytes, polystyrene sulfonate), biological membranes, cellular components, and globular proteins are electrically charged. Electrostatic interactions in biological systems are therefore of great importance for understanding of interactions between charged molecules and membrane surfaces.

Examples of electrically charged systems from biology include also self-assembling dispersions such as spherical inverse micelles, phospholipid vesicles, and microemulsions [1,2]. Such objects are formed by aggregation of amphiphilic molecules in a way that the hydrophilic parts of the molecules are in contact with electrolyte solution, while the hydrophobic parts avoid such contact. Micelles are small aggregates of amphiphilic molecules in aqueous solutions. Microemulsions are formed in mixtures of amphiphiles, water and oil, where domains of water (in oil) or oil (in water) are separated by surfactant monolayers. Multilamellar vesicles can then be formed by several surfactant bilayers separating an internal compartment from the continuous phase of the solution.

In biological medium (ionic solution) free ions are always present. The charges of ions and molecules are multiples of elementary charge. Multivalent ions are commonly treated as point charges. However, real ions (and particularly organic *nanoparticles*) often possess an internal structure with the individual charges being located at distinct, well-separated positions [3–5]. Among others [6], a characteristic example is the rod-like backbone structure of various DNA condensing agents such as the three- and tetra-valent ions spermine and spermidine, different proteins [7], protamine sulfate, or poly-lysine.

As already mentioned, some of the constituents of the biological membranes are ionized and therefore the biological membranes are electrically charged. The membrane charge, its spatial distribution, and the spatial distribution of ions in the

solution in the close proximity of the inner and outer membrane surfaces determine the profile of electric potential across the membrane [8,9]. The electrically charged molecular groups on both membrane surfaces protrude into the solution phase and therefore the inner and outer membrane surface potentials are smaller in comparison with the situation where the charge would be distributed in the planes of both membrane surfaces [9,10]. Nevertheless, for the sake of simplicity the electric charge distribution of membrane surfaces is usually described by effective surface charge characterized by the surface charge density σ.

Recently, much attention is devoted to inorganic and organic hollow bilayer membrane cylindrical structures in the nanometer range. Among other systems, nanotubes have been found in different phospholipid systems [11,12]. In cellular systems a direct transport between different cells or cellular organelles has been observed through hollow nanotubes or by carrier vesicles guided by nanotubes [13–15]. In membrane nanotubes, the walls of organic nanotubes are usually charged and are in contact with electrolyte solution [16]. Ion channels or pores in biological membranes and blood capillaries are also examples of cylindrical nanotubes.

The *electric double layer* is composed of a charged surface and the electrolyte solution is in contact with the charged surface.

The distribution of the ions in the electrolyte solution close to the charged surface is given by the competition between the electrostatic interactions and the entropy of the ions in the solution. Owing to the electrostatic forces between the charged surface and the ions in the solution, the counter-ions (the ions with the charge of the opposite sign than the charged surface) are accumulated close to the surface and the coions (the ions with the charge of the same sign than the surface) are depleted from the surface. A diffuse electric double layer influences the overall electrostatic interaction of the charged surface with its environment as well as the internal properties of the membrane carrying the surface charge. With respect to the geometry we distinguish planar [8], cylindrical [17–19], spherical [20], and other electric double layers.

The electric double layer has been a subject of extensive study since the pioneering work of Gouy [21] and Chapman [22]. The ions within the so-called Poisson–Boltzmann theory [1,2,8] were treated as dimensionless, while the electrolyte solution was accounted for by a uniform dielectric constant. The charged surfaces were considered as uniformly charged (see also [8–10]).

The improvement of the Gouy–Chapman theory can be obtained by including the direct ion–ion interactions. The fluctuation potential [23] due to the self-atmosphere of ion and the ion–ion exclusion volume term were taken into account in the modified Poisson–Boltzmann equation [24–26]. The integral equation methods, such as the hypernetted chain (HNC) approximation, have also been carried out [27–31]. Many different attempts have been made to incorporate steric effects into the PB equation. Freise [32] introduced the excluded volume effect by a pressure-dependent potential, while Wicke and Eigen [33] used a thermodynamic approach, multiplying the numerical density of ions by a factor containing the number of the vacant sites. More recently, the finite size of particles has been incorporated into the PB theory in a transparent way, based on a lattice statistics model [34–37], by using functional density approaches [38–40] and by a model including the surface charge

correlations, where the ions and solvent molecules were treated as hard spheres [41]. Monte Carlo simulations incorporate the direct interactions between ions and interactions between the ions and charged surfaces [24–26,42,43]. With the Monte Carlo technique it is possible to obtain numerically exact data and compare these data with the approximate theories. The advanced approaches [43] and the hypernetted chain integral equations [44,27] lead to a better agreement with Monte Carlo (MC) simulations for divalent counter-ions.

The Poisson–Boltzmann (PB) theory is a widely used mean-field level method to calculate interactions between charged surfaces in aqueous solution of counter-ions and coions. For monovalent salt, its predictions are generally found to agree well with experimental results and computer simulations. However, the presence of *multivalent* ions can affect the nature of the interactions between charged surfaces in a way that qualitatively differs from the PB prediction. A remarkable example is the possibility of *attraction* between two identical, like-charged surfaces that the mean-field Poisson–Boltzmann approach is unable to predict. This attraction receives much interest [45] because it is observed in several biologically relevant processes such as condensation of DNA [46], network formation in actin solutions [47], virus aggregation [48], and interactions between like-charged lipid membranes that occur during adhesion [7] and fusion. Various theoretical approaches ascribe this attraction to the presence of the direct ion–ion correlations [49,50]. An intuitive understanding of these correlations can be based on the formation of a periodic counter-ion arrangement in the vicinity of each macroion, similar to a Wigner crystal. The two inter-locked counter-ion-decorated charged surfaces then experience a short-range attraction. However, Linse [51] has shown that correlation attraction occurs even if no Wigner crystal arrangement is present.

The Monte Carlo (MC) simulations of Guldbrand *et al.* [52] first confirmed the existence of attraction between equally charged surfaces immersed into the solution composed of quadrupolar (divalent) ions in the limit of high surface charge density, which were originally predicted by Oosawa [18]. The anisotropic hypernetted chain approximation within the primitive electrolyte model for divalent ions was used [53,54], where the ions are described as charged hard spheres immersed in a dielectric continuum. Attractive interaction between identical, like-charged surfaces in aqueous solution composed of short divalent rod-like ions was predicted [3].

Here we present a statistical mechanical approach to the functional density theory of the electric double layer. First, in the mean filed approximation the consistently related free energy, ion distribution function, and differential equation for the electrostatic potential were obtained. We upgrade the description of the Poisson–Boltzmann theory by considering the effect of the size of ions (i.e., charged nanoparticles). The influence of the ion size on the properties of the electric double layer is discussed. The effective thickness of electric double layer in different geometries is derived. Further, we formulate a description of a solution composed of large charged nanoparticles with spatially distributed charge. We discuss the interaction between two charged surfaces immersed in the solution of charged nanoparticles (quadrupolar or dipolar) with spatially distributed internal charge [5] (see also Fig. 1).

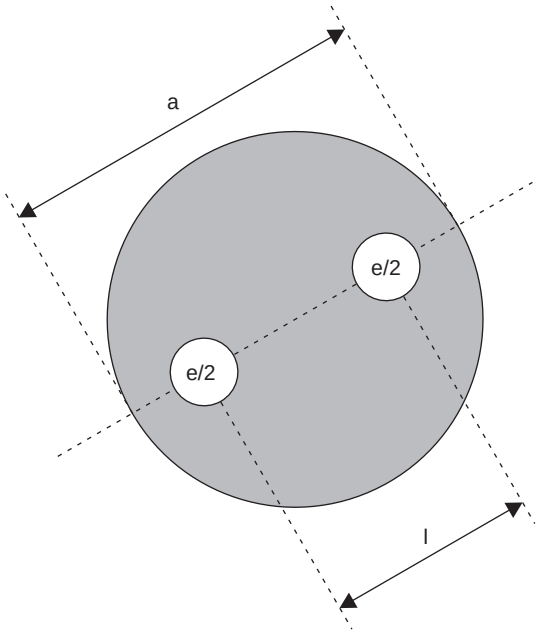

Figure 1 Schematic figure of a large spheroidal multivalent ion with net electric charge e and average diameter a. In the model the space charge distribution of the multivalent ion is described by two effective poly-ions of charge $e/2$ located at different well-separated positions (i.e., at the distance $l \leq a$). The main axis of the ion coincides with the line connecting the two poly-ions.

2. Electrostatic Free Energy

2.1. Electrostatic Energy

The distribution of ions in the electric double layer reflects a balance between electrostatic interactions and entropy. First we consider the electrostatic interactions. The Poisson equation expresses the general relation between the charge distribution and the electrostatic potential. It follows from the Gauss law $\nabla \cdot \mathbf{E} = \rho / \varepsilon \varepsilon_0$ in which we insert the definition of the electrostatic potential $\mathbf{E} = -\nabla \Phi$ [55] so that

$$\nabla^2 \Phi = -\frac{\rho}{\varepsilon \varepsilon_0} \tag{1}$$

where ∇^2 is the Laplace operator, ∇ is the nabla operator, $\mathbf{E}$ is the electric field strength, ε is the dielectric constant, and ε_0 is the permittivity of the free space. From a given space charge distribution $\rho\,(x, y, z)$, the electrostatic potential $\Phi(x, y, z)$ can be calculated provided the conditions to be satisfied at geometrical boundaries.

The electrostatic energy of the system can be expressed as an integral of the square of the electric field strength over the system [55]:

$$F_{\mathrm{el}} = \frac{1}{2}\int \varepsilon\varepsilon_0 E^2 \mathrm{d}V. \tag{2}$$

If the system possesses the radial symmetry then the electrostatic energy can be written as

$$F_{\mathrm{el}} = \frac{1}{2}\int \varepsilon\varepsilon_0 \left(\frac{\mathrm{d}\Phi}{\mathrm{d}r}\right)^2 J(r)\mathrm{d}r, \tag{3}$$

where r is the radial coordinate in cylindrical and spherical geometry, while in the planar geometry r denotes the distance from the charged plane in the direction perpendicular to the plane. $J(r)$ is defined as

$$\begin{aligned} J(r) &= A \quad \text{in planar geometry,} \\ J(r) &= 2\pi r l \quad \text{in cylindrical geometry,} \\ J(r) &= 4\pi r^2 \quad \text{in spherical geometry} \end{aligned} \tag{4}$$

where in the planar geometry A denotes the area of the charged surface, while l is the elongation of the cylinder.

2.2. Entropy

2.2.1. Solution of counter-ions

We consider the entropy of the system composed of only a finite size counter-ions (nanoparticles) . The lattice model is used (Fig. 2).

The system is divided into cells of equal volume ΔV. In a particular cell chosen, there are N counter-ions. The excluded volume effect is taken into account in the description by considering that the counter-ions are distributed over M lattice sites. The number of spatial arrangements of N non-interacting counter-ions in a small cell with M lattice sites is

$$W = \frac{M(M-1)(M-2)\ldots(M-(N-1))}{N!} \tag{5}$$

and can be rewritten into

$$W = \frac{M!}{N!(M-N)!}. \tag{6}$$

The configurational entropy of the cell S_{cell} can be computed by using the Boltzmann equation [56]

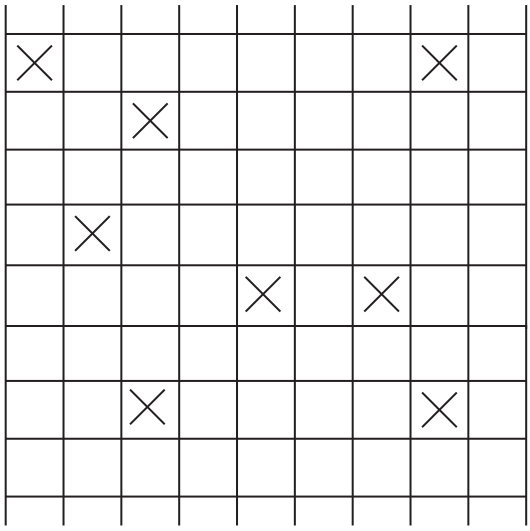

Figure 2 Schematic presentation of the lattice model, only counter-ions are included.

$$S_{\text{cell}} = k \ln W \tag{7}$$

where k is the Boltzmann constant. Using the Stirling's approximation for large N: $\ln N! \simeq N \ln N - N$ we get for $\ln W$:

$$\begin{aligned} \ln W =& M \ln M - M - N \ln N + N - (M - N) \\ & \ln (M - N) + (M - N). \end{aligned} \tag{8}$$

The redistribution of the terms in Eq. (8) gives

$$\begin{aligned} \ln W &= M \ln M - N \ln N - (M - N) \ln \left(M \left(1 - \frac{N}{M} \right) \right) \\ &= M \ln M - N \ln N - (M - N) \ln M - (M - N) \ln \left(1 - \frac{N}{M} \right) \\ &= -N \ln N + N \ln M - (M - N) \ln \left(1 - \frac{N}{M} \right). \end{aligned} \tag{9}$$

After the summation of the first and the second term in Eq. (9) we get

$$\ln W = -N \ln \left(\frac{N}{M} \right) - (M - N) \ln \left(1 - \frac{N}{M} \right). \tag{10}$$

By inserting Eq. (10) into Eq. (7) we get the expression for the entropy of a single cell

$$S_{\text{cell}} = -k\left(N \ln \frac{N}{M} + (M-N) \ln \left(1 - \frac{N}{M}\right)\right). \tag{11}$$

In the following we introduce the volume of a single counter-ion (nanoparticle) υ_0. The volume of the cell with M lattice sites is then given by $\Delta V = M\,\upsilon_0$. The entropy of the whole system can be thus obtained by the integration of entropy over all cells of the system:

$$S = \int S_{\text{cell}} \frac{\mathrm{d}V}{\Delta V}, \tag{12}$$

where S_{cell} is given by Eq. (11). We insert Eq. (11) into Eq. (12) and get

$$S = -k \int \left[n \ln (n\upsilon_0) + \frac{1}{\upsilon_0}(1 - n\upsilon_0) \ln (1 - n\upsilon_0)\right] \mathrm{d}V, \tag{13}$$

where the number density of counter-ions is defined by $n = N/\Delta V$ and $\upsilon_0 = \Delta V/M$. Equation (13) takes into account the finite size of counter-ions and coions (nanoparticles). If we assume a very dilute system ($n\,\upsilon_0 \ll 1$ everywhere in the solution) the second term in Eq. (13) can be approximated by $\ln(1 - n\,\upsilon_0) \approx -n\,\upsilon_0$, where we have neglected quadratic and higher order terms. In the limit of very dilute system the entropy (Eq. 13) becomes

$$S = -k \int [n \ln (n\upsilon_0) - n] \mathrm{d}V. \tag{14}$$

The entropic contribution to the free energy $F_{\text{ent}} = -TS$ can be therefore expressed as [2]

$$F_{\text{ent}} = kT \int [n \ln (n\upsilon_0) - n] \mathrm{d}V, \tag{15}$$

where T is the absolute temperature.

2.2.2. Solution of counter-ions and coions

We consider now the entropy of the solution composed of counter-ions and coions. The finite sizes of ions (nanoparticles) are again considered within the lattice model (Fig. 3).

The system is divided into cells of equal volume ΔV. In the particular cell chosen, there are N_+ counter-ions and N_- coions. The number of spatial arrangements of non-interacting counter-ions and coions in small cell with M lattice sites is (see Fig. 3):

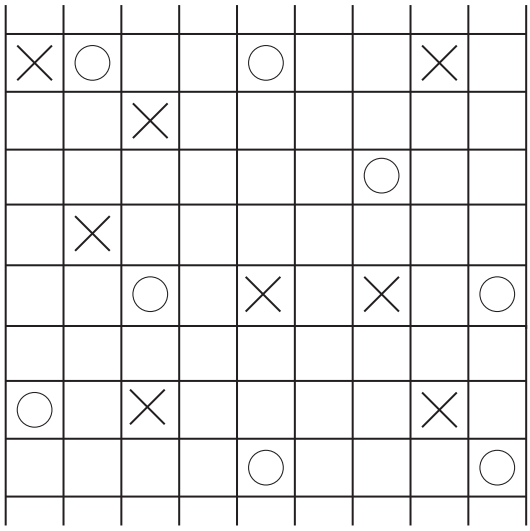

Figure 3 Schematic presentation of the lattice model, counter-ions (×) and coions (○) are included.

$$W = \frac{M(M-1)(M-2)\ldots(M-(N-1))}{N_+!N_-!} \tag{16}$$

and can be rewritten into

$$W = \frac{M!}{N_+!N_-!(M-N)!}, \tag{17}$$

where

$$N = N_+ + N_-. \tag{18}$$

The translational entropy of the mixed system of the single cell S_{cell} is then [56]

$$S_{\text{cell}} = k \ln W \tag{19}$$

Using the Stirling's approximation for large N_i : $\ln N_i! \simeq N_i \ln N_i - N_i$, $i = \{+, -\}$, the expression for $\ln W$ transforms into:

$$\begin{aligned} \ln W = M \ln M - M - N_+ \ln N_+ + N_+ - N_- \ln N_- + N_- \\ - (M-N) \ln (M-N) + (M-N). \end{aligned} \tag{20}$$

The redistribution of the terms in Eq. (20) gives

$$\ln W = -N_+ \ln \left(\frac{N_+}{M}\right) - N_- \ln \left(\frac{N_-}{M}\right) - (M-N) \ln \left(1 - \frac{N}{M}\right). \tag{21}$$

To simplify calculations we assume in the following that counter-ions and coions have the same volume υ_0. The volume of the cell with M sites is then given by $\Delta V = M\,\upsilon_0$. The number density of counter-ions is defined as

$$n_+ = N_+/\Delta V, \tag{22}$$

while the number density of coions is

$$n_- = N_-/\Delta V. \tag{23}$$

The configurational entropy of the whole system is obtained by the integration over all cells of the system:

$$S = \int S_{\text{cell}} \frac{\mathrm{d}V}{\Delta V} \tag{24}$$

where S_{cell} is given by Eq. (19). We insert Eq. (21) into Eq. (19) to get

$$\begin{aligned} S = -k \int [&n_+ \ln (n_+\upsilon_0) + n_- \ln (n_-\upsilon_0) \\ &+ \frac{1}{\upsilon_0}(1 - n_+\upsilon_0 - n_-\upsilon_0) \ln (1 - n_+\upsilon_0 - n_-\upsilon_0)]\mathrm{d}V \end{aligned} \tag{25}$$

Equation (25) takes into account the finite size of counter-ions (nanoparticles). If we assume that $(n_+ + n_-)\,\upsilon_0 \ll 1$ everywhere in the solution then the second term in Eq. (25) can be approximated by

$$\ln (1 - n_+\upsilon_0 - n_-\upsilon_0) \approx -(n_+ + n_-)\upsilon_0 \tag{26}$$

where we neglected the quadratic and higher order terms. The entropy (Eq. (25)) thus becomes

$$S = -k \int [n_+ \ln (n_+\upsilon_0) - n_+ + n_- \ln (n_-\upsilon_0) - n_-]\mathrm{d}V \tag{27}$$

The entropic part of the free energy $\tilde{F}_{\text{ent}} = -TS$ is therefore

$$\tilde{F}_{\text{ent}} = kT \int \sum_{i=+,-} [n_i \ln (n_i\upsilon_0) - n_i]\mathrm{d}V \tag{28}$$

where the sum runs over counter-ions and coions. From the expression for the configurational free energy (Eq. (28)) we need to subtract the reference free energy, i.e., the translational free energy of the system with vanishing electrostatic potential. We assume that the bulk (where the electrostatic potential is zero) number densities of counter-ions (n_{+0}) and coions (n_{-0}) are equal

$$n_0 = n_{+0} = n_{-0} \tag{29}$$

The difference between the entropic part of the free energy $F_{\text{ent}} \sim$ and the reference entropic part of the free energy F_{ref} is then:

$$\tilde{F}_{\text{ent}} - F_{\text{ref}} = kT \sum_{i=+,-} \int [n_i \ln (n_i \upsilon_0) - n_i] \mathrm{d}V - 2kT \int [n_0 \ln (n_0 \upsilon_0) - n_0] \mathrm{d}V. \quad (30)$$

By taking into account the relation

$$\int dV [2n_0 - \sum_{i=+,-} n_i] = 0 \quad (31)$$

we Eq. (30) into:

$$\tilde{F}_{\text{ent}} - F_{\text{ref}} = kT \sum_{i=+,-} \int [n_i \ln (n_i \upsilon_0) - n_i] \mathrm{d}V - 2kT \int [n_0 \ln (n_0 \upsilon_0) - n_0] \mathrm{d}V - kT \sum_{i=+,-} \int n_i \ln (n_0 \upsilon_0) \mathrm{d}V + kT \int 2n_0 \ln (n_0 \upsilon_0) \mathrm{d}V. \quad (32)$$

Note that the validity of the Eq. (31) implies that the sum of the last two terms in Eq. (32) is zero, where it is taken into account that $\ln(n_0 \upsilon_0) = \text{const}$. After some calculation we get from Eq. (32) the entropic part of the free energy for the solution composed of counter-ions and coions $F_{\text{ent}} = \tilde{F}_{\text{ent}} - F_{\text{ref}}$ in the form (see also [34])

$$F_{\text{ent}} = kT \sum_{i=+,-} \int \left[n_i \ln \left(\frac{n_i}{n_0} \right) - (n_i - n_0) \right] \mathrm{d}V. \quad (33)$$

In the derivation of Eq. (33) we assumed that $(n_+ + n_-)\, \upsilon_0 \ll 1$ everywhere in the solution. In the following the assumption $(n_+ + n_-)\, \upsilon_0 \ll 1$ will be abandoned and the entropic part of the free energy $\tilde{F}_{\text{ent}} = -TS$ will be calculated directly from the Eq. (25) without any additional simplifications:

$$\tilde{F}_{\text{ent}} = kT \int \left[\sum_{i=+,-} n_i \ln (n_i \upsilon_0) + \frac{1}{\upsilon_0} \left(1 - \sum_{i=+,-} n_i \upsilon_0 \right) \ln \left(1 - \sum_{i=+,-} n_i \upsilon_0 \right) \right] \mathrm{d}V. \quad (34)$$

Similarly as in Eq. (30) we need to subtract the reference free energy. The difference between the entropic part of the free energy $\tilde{F}_{\text{ent}}$ and the reference entropic part of the free energy F_{ref} is thus

$$\begin{aligned}\tilde{F}_{\text{ent}} - F_{\text{ref}} = kT \int \mathrm{d}V \left[\sum_{i=+,-} n_i \ln (n_i \upsilon_0) - 2n_0 \ln (n_0 \upsilon_0) \right] + \\ + kT \int \mathrm{d}V \frac{1}{\upsilon_0} \left(1 - \sum_{i=+,-} n_i \upsilon_0 \right) \ln \left(1 - \sum_{i=+,-} n_i \upsilon_0 \right) - \\ - kT \int \mathrm{d}V \frac{1}{\upsilon_0} (1 - 2n_0 \upsilon_0) \ln (1 - 2n_0 \upsilon_0). \end{aligned} \tag{35}$$

By taking into account the relation (31) we transformed Eq. (35) into:

$$\begin{aligned}\tilde{F}_{\text{ent}} - F_{\text{ref}} = kT \int \mathrm{d}V \Bigg\{ \sum_{i=+,-} n_i \ln (n_i \upsilon_0) - 2n_0 \ln (n_0 \upsilon_0) \\ - \sum_{i=+,-} n_i \ln (n_0 \upsilon_0) + 2n_0 \ln (n_0 \upsilon_0) \\ + \frac{1}{\upsilon_0} \left(1 - \sum_{i=+,-} n_i \upsilon_0 \right) \ln \left(1 - \sum_{i=+,-} n_i \upsilon_0 \right) \\ - \frac{1}{\upsilon_0} (1 - 2n_0 \upsilon_0) \ln (1 - 2n_0 \upsilon_0) - \\ - \frac{1}{\upsilon_0} \left(1 - \sum_{i=+,-} n_i \upsilon_0 \right) \ln (1 - 2n_0 \upsilon_0) \\ + \frac{1}{\upsilon_0} (1 - 2n_0 \upsilon_0) \ln (1 - 2n_0 \upsilon_0) \Bigg\}. \end{aligned} \tag{36}$$

By taking into account Eq. (36), $\ln(n_0 \upsilon_0) = \text{const}$, and $\ln(1–2n_0 \upsilon_0) = \text{const}$, we get the entropic part of the free energy

$$\begin{aligned} F_{\text{ent}} = \tilde{F}_{\text{ent}} - F_{\text{ref}} = +kT \int \mathrm{d}V \sum_{i=+,-} n_i \ln \left(\frac{n_i}{n_0} \right) \\ + kT \int \mathrm{d}V \left(\frac{1}{\upsilon_0} - \sum_{i=+,-} n_i \right) \ln \left(\frac{\frac{1}{\upsilon_0} - \sum_{i=+,-} n_i}{\frac{1}{\upsilon_0} - 2n_0} \right). \end{aligned} \tag{37}$$

In our model the volume of a single nanoparticle (υ_0) is equal to the volume of one lattice site

$$n_{\text{s}} = \frac{1}{\upsilon_0} = \frac{1}{a^3} \tag{38}$$

where we define a as a lattice constant. All lattice sites are occupied by either solvent molecules or nanoparticles (ions), therefore

$$n_s = n_w + \sum_{j=+,-} n_j \tag{39}$$

where n_w is the number density of lattice sites occupied by solvent (water) molecules. Different values of the lattice constant a describe different sizes of the ions (nanoparticles). In the following the number densities of counter-ions and coions are referred to as the respective concentrations. By taking Eq. (38) into account we may rewrite Eq. (37) in the following form:

$$\begin{aligned} F_{ent} = kT \int dV \sum_{i=+,-} n_i \ln\left(\frac{n_i}{n_0}\right) \\ + kT \int dV (n_s - \sum_{i=+,-} n_i) \ln\left(\frac{n_s - \sum_{i=+,-} n_i}{n_s - 2n_0}\right). \end{aligned} \tag{40}$$

2.3. Functional Density Theory of Electric Double Layer

In the described model of electric double layer the charged surface is assumed to carry an uniformly distributed charge with the surface charge density σ. The solution is composed of solvent molecules and nanoparticles. The nanoparticles are in general counter-ions and/or coions. We restrict our consideration to the planar, cylindrical, and spherical electric double layers. The geometry of cylindrical surface is described by the radius of curvature r_0 and length l, the spherical surface is described by the radius of curvature r_0 (Figs. 4 and 5).

In the non-planar geometry the electric field must vanish far from the charged surface in the convex case and at the cylinder axis or at the centre of the sphere in the concave case.

The electrostatic interactions are described within the mean field approximation while the finite size of the nanoparticles in the solution is considered by means of excluded volume effect. The latter is taken into account within a statistical mechanical description as described in the previous section, where each particle in the solution occupies one and only one site of a finite volume [34,35].

2.3.1. Solution of counter-ions only

2.3.1.1. Single double layer We consider a system composed of a charged surface and a solution of counter-ions only. The solvent (water) molecules are accounted for by a uniform dielectric constant $\varepsilon \sim 78.5$ and by the excluded volume principle.

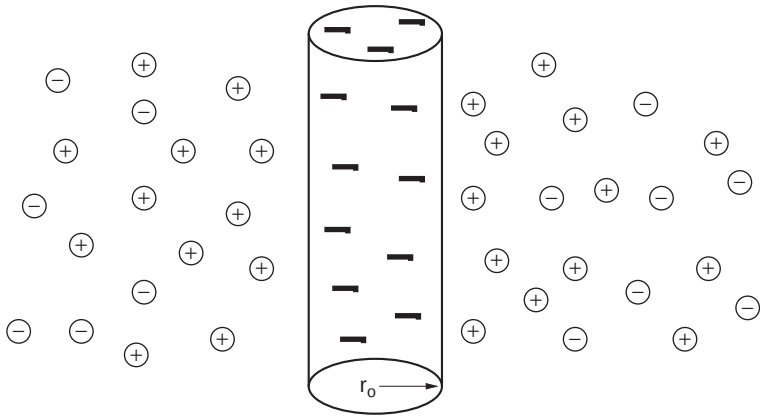

Figure 4 Schematic presentation of a cylindrical electric double layer outside the tube with radius r_o and surface charge density σ_o. The counter-ions are accumulated near the charged surface while the coions are depleted from the vicinity of the charged surface [57].

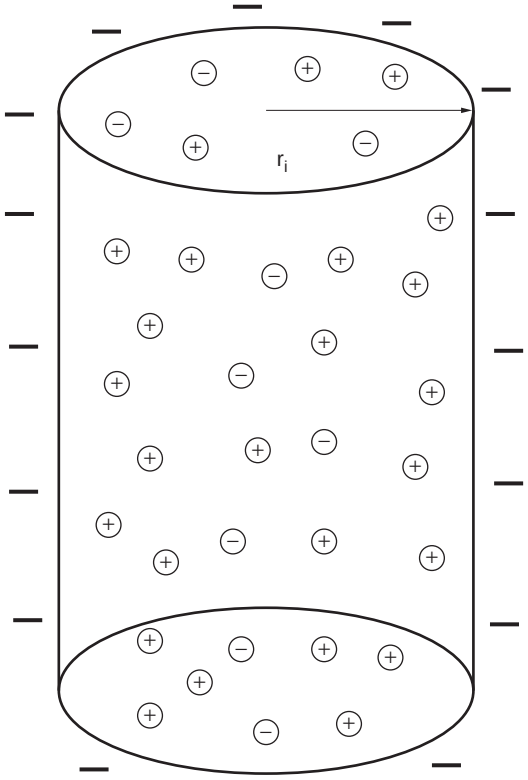

Figure 5 Schematic presentation of a cylindrical electric double layer inside the tube with radius r_i and surface charge density σ_i. The counter-ions are accumulated near the charged surface while the coions are depleted from the vicinity of the charged surface.

The electrostatic free energy of the system can be written as a sum of electrostatic energy (Eq. (3)) and the entropic contribution to the free energy (Eq. (13)):

$$F = \frac{1}{2}\varepsilon\varepsilon_0 \int_{r_0}^{R} E^2(r) J(r) \mathrm{d}r + kT \int_{r_0}^{R} J(r) \left[n(r) \ln \left(n(r)\upsilon_0 + \frac{1}{\upsilon_0}(1 - n(r)\upsilon_0) \ln \left(1 - n(r)\upsilon_0\right) \right] \mathrm{d}r. \tag{41}$$

where $E(r)$ is the electric field strength, $n(r)$ is the counter-ion concentration, and $J(r)$ is defined by Eq. (4). In cylindrical and spherical geometry, r_0 denotes the radius of the charged cylindrical or spherical surface, while in the planar geometry $r_0 = 0$. In the planar geometry and in the convex cylindrical and spherical geometry $R \to \infty$, while in concave cylindrical and spherical geometry $R = 0$. In the cylindrical and spherical geometries the electrostatic field depends on the radial coordinate r. In the planar geometry r denotes the distance from the charged plane in the direction perpendicular to the plane.

The free energy of the whole system, subject to the local thermodynamic equilibrium, is

$$F = \int_{r_0}^{R} f(E(r), n(r)) J(r) \mathrm{d}r, \tag{42}$$

where the density of the free energy is given by

$$f(E(r), n(r)) = \frac{1}{2}\varepsilon\varepsilon_0 E^2(r) + kT \left[n(r) \ln \left(n(r)\upsilon_0 \right) + \frac{1}{\upsilon_0}(1 - n(r)\upsilon_0) \ln \left(1 - n(r)\upsilon_0\right) \right]. \tag{43}$$

The counter-ion concentration $n(r)$ and the electric field strength are not known in advance. Thus, in the following, explicit expressions for $n(r)$ and $E(r)$ are obtained using the condition of the free energy to be at its minimum at thermodynamic equilibrium of the whole system. The condition for the global equilibrium

$$\delta F = 0 \tag{44}$$

is subject to [34] the followings:

- the global constraint requiring the electro-neutrality of the whole system

$$\int_{r_0}^{R} n(r) J(r) \mathrm{d}r - \frac{\sigma A}{Ze_0} = 0, \tag{45}$$

- the local constraint requiring the validity of the differential form of the Gauss's law $\varepsilon\varepsilon_0 \nabla \cdot \mathbf{E} = \rho\,(r)$, where $\rho\,(r) = e_0 \upsilon Z n(r)$ is the volume charge density and

$$\varepsilon\varepsilon_0 \frac{1}{r^\alpha} \frac{\partial (r^\alpha E(r))}{\partial r} - e_0 Z n(r) = 0, \tag{46}$$

where in the planar geometry $\alpha = 0$, in the spherical geometry $\alpha = 2$ while in the cylindrical geometry $\alpha = 1$ and Z is the valency of counter-ions.

The method of undetermined multipliers [34,57,58] is used to determine the extreme of the free energy (42) taking into account the constraints (45) and (46). The variational problem can be expressed by the Euler–Lagrange equations

$$\frac{\partial L^*}{\partial E} - \frac{\mathrm{d}}{\mathrm{d}r}\left(\frac{\partial L^*}{\partial\left(\frac{\partial E}{\partial r}\right)}\right) = 0 \tag{47}$$

$$\frac{\partial L^*}{\partial n} = 0 \tag{48}$$

where

$$L^*\ (\ E(r), n(r), \frac{\partial E(r)}{\partial r}, \eta(r)\ ) = J(r) * \left[f(E(r), n(r)) + \mu n(r) - \eta(r)\left(\varepsilon\varepsilon_0 \frac{1}{r^\alpha} \frac{\partial (r^\alpha E(r))}{\partial r} - e_0 Z n(r)\right)\right]$$

μ is the global Lagrange multiplier, while $\eta(r)$ is the local Lagrange multiplier. The local Lagrange multiplier $\eta(r)$ can be expressed from the Euler–Lagrange Eq. (47):

$$\eta(r) = \Phi(r) \tag{49}$$

where we took into account that $\mathbf{E} = -\nabla\Phi$, while it follows from the Euler–Lagrange Eq. (48) that

$$kT[\ \ln\ (n\upsilon_0) - \ \ln\ (1 - n\upsilon_0)] + \mu + e_0 Z\eta(r) = 0. \tag{50}$$

From Eqs. (49) and (50) the counter-ion distribution function is obtained:

$$n(r) = \frac{1}{\upsilon_0} \times \frac{1}{1 + e^{(\mu + e_0 Z\Phi(r))/kT}}, \tag{51}$$

where the Lagrange multiplier μ can be determined from the condition of electroneutrality (Eq. (45)). The Gauss law (Eq. (46)) and the particle distribution functions (Eq. (51)) give the differential equation for the electrostatic potential $\Phi(r)$:

$$\frac{\mathrm{d}^2\Phi(r)}{\mathrm{d}r^2} + \frac{\alpha}{r}\frac{\mathrm{d}\Phi(r)}{\mathrm{d}r} = -\frac{e_0 Z}{\varepsilon\varepsilon_0 \upsilon_0} \frac{1}{1 + e^{(\mu + e_0 Z\Phi(r))/kT}} \tag{52}$$

In the following the Lagrange multiplier μ is expressed from Eq. (51) as a function of concentration of counter-ions (nanoparticles) for $\Phi = 0$:

$$e^{\mu/kT} = \frac{1}{(n_0/n_s)} - 1, \tag{53}$$

where the number density of the lattice sites is $n_s = 1/v_0$ (see Eq. (38)). In the limit of very dilute system ($n_0/n_s \ll 1$) Eq. (53) becomes

$$e^{\mu/kT} \simeq \frac{1}{(n_0/n_s)}. \tag{54}$$

Taking into account the approximative expression (54) we can transform Eq. (51) to the form of the Boltzmann distribution function:

$$n(r) = \frac{n_s}{1 + (n_s/n_0)e^{e_0 Z\Phi(r)/kT}} \simeq n_0 e^{-e_0 z\Phi(r)/kT} \tag{55}$$

In accordance, also the Eq. (52) transforms into the so-called Poisson–Boltzmann equation:

$$\frac{d^2\Phi(r)}{dr^2} + \frac{\alpha}{r} \times \frac{d\Phi(r)}{dr} = -\frac{e_0 Z}{\varepsilon\varepsilon_0} n_0 e^{-Ze_0\Phi(r)/kT.} \tag{56}$$

The condition of electro-neutrality of the whole system (Eq. (45)) is equivalent to two boundary conditions. The first boundary condition states that the electric field is zero far from the charged surface:

$$\left.\frac{d\Phi(r)}{dr}\right|_{r=R} = 0, \tag{57}$$

where $R \to \infty$, while the second boundary condition (at the interface) is:

$$\left.\frac{d\Phi(r)}{dr}\right|_{r=r_0} = -\frac{\sigma}{\varepsilon\varepsilon_0}. \tag{58}$$

In the planar geometry r denotes the distance from the charged plane in direction perpendicular to the plane, therefore in Eq. (58) $r_0 = 0$ for planar geometry.

2.3.1.2. Two interacting double layers In the following we shall consider a system composed of two flat and equally uniformly charged surfaces immersed in an aqueous solution composed of counter-ions only (Fig. 6). The surface charge density of each surface is σ. The first charged surface is located at $x = 0$ ($r_0 = 0$), while the second charged surface is located at $x = D$ ($R = D$), where $x \equiv r$ is the coordinate

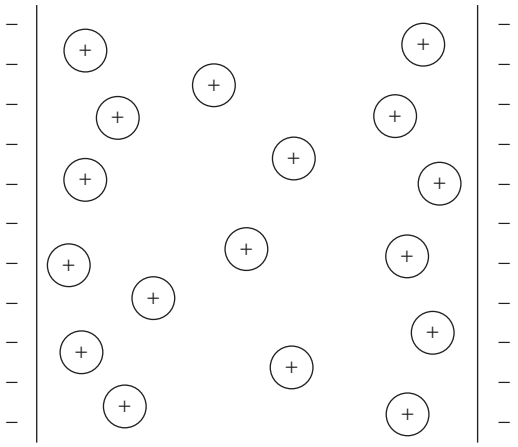

Figure 6 Two flat and equally charged surfaces immersed in aqueous solution composed of counter-ions only.

perpendicular to the charged surfaces. The distance between the charged surfaces is D. Assuming the symmetry of the system with respect to the plane $x = D/2$, the boundary conditions (76) and (58) should be replaced by

$$\left.\frac{\mathrm{d}\Phi(x)}{\mathrm{d}x}\right|_{x=0} = -\frac{\sigma}{\varepsilon\varepsilon_0}, \tag{59}$$

$$\left.\frac{\mathrm{d}\Phi(x)}{\mathrm{d}x}\right|_{x=\frac{D}{2}} = 0. \tag{60}$$

The electrostatic potential $\Phi(x)$ is calculated by numerically solving the Eq. (56), taking into account the boundary conditions (59) and (60). Then the concentration of counter-ions $n(x)$ is determined by using Eq. (55). Finally, the electrostatic free energy of the system is calculated in the limit of very dilute solution (see also Eq. (15));

$$F/A = \frac{1}{2}\varepsilon\varepsilon_0 \int_0^D \left(\frac{\mathrm{d}\Phi}{\mathrm{d}x}\right)^2 \mathrm{d}x + kT \int_0^D [n(x)\ \ln\ (n(x)\upsilon_0) - n(x)]\mathrm{d}x. \tag{61}$$

Figure 7 shows the electrostatic free energy F (full line) as a function of the distance between the equally charged planar surfaces D. We see that the free energy F decreases with increasing distance between the surfaces D, which corresponds to the repulsive force between equally charged surfaces. This is the consequence of decreasing entropic contribution to the free energy, which prevails over the increase of the electrostatic part of the free energy with increasing D.

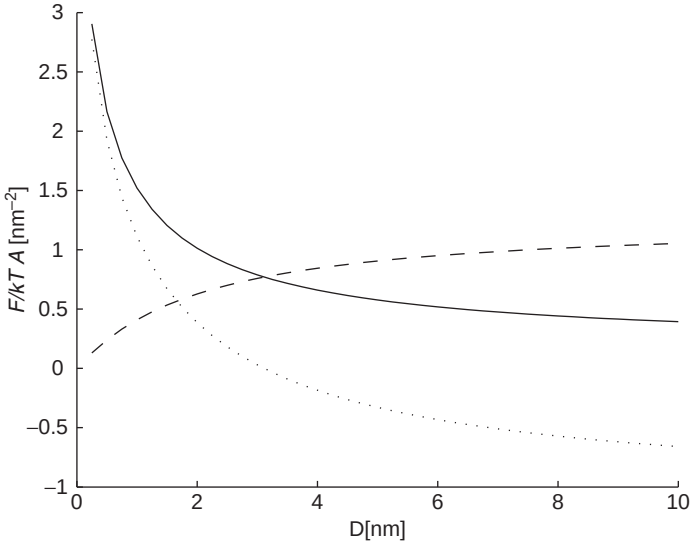

Figure 7 Free energy (full line), electrostatic energy (dashed line) and configurational entropy (dotted line) of a system with counter-ions only as a function of the distance between the equally charged surfaces D. Model parameters are $|\sigma| = 0.1$ As/m^2 and $\upsilon_0 = 5$ nm^3.

2.3.2. Solution of counter-ions and coions

Electrostatic free energy of the system composed of counter-ions and coions is derived from Eq. (3) and (40) [34,57,56]:

$$\begin{aligned} F = & \frac{1}{2}\varepsilon\varepsilon_0 \int_{r_0}^{R} E^2(r) J(r) \mathrm{d}r \\ & + kT \sum_{j=+,-} \int_{r_0}^{R} J(r) n_j(r) \ln\left(\frac{n_j(r)}{n_0}\right) \mathrm{d}r \\ & + kT \int_{r_0}^{R} J(r) \left(n_s - \sum_{j=+,-} n_j(r)\right) \ln\left(\frac{n_s - \sum_{j=+,-} n_j(r)}{n_s - 2n_0}\right) \mathrm{d}r, \end{aligned} \tag{62}$$

where n_+ is concentration of counter-ions, n_- is concentration of coions, n_0 is the bulk concentration of counter-ions and of coions, n_s is defined by Eqs. (38) and (39) and $J(r)$ is given by Eq. (4).

The free energy of the whole system, subject to the local thermodynamic equilibrium, is

$$F = \int_{r_0}^{R} f(E(r), n_+(r), n_-(r)) J(r) \mathrm{d}r, \tag{63}$$

where the density of the free energy is given by

$$f(E(r), n_+(r), n_-(r)) = \frac{1}{2}\varepsilon\varepsilon_0 E^2(r) + kT\sum_{j=+,-} n_j(r)\ \ln\left(\frac{n_j(r)}{n_0}\right) + kT\left(n_s - \sum_{j=+,-} n_j(r)\right)\ \ln\left(\frac{n_s - \sum_{j=+,-} n_j(r)}{n_s - 2n_0}\right)\mathrm{d}r \tag{64}$$

The particle distribution functions $n_+(r)$ and $n_-(r)$ and the electric field strength $E(r)$ are obtained by using the condition of the free energy to be at its minimum at thermodynamic equilibrium of the whole system. The condition for the global equilibrium

$$\delta F = 0 \tag{65}$$

is subject to the following [34]:

- The global constraint requiring that the total number of particles of each species per volume of the whole system, Λ_j, is constant

$$\int_{r_0}^{R} (n_j(r) - \Lambda_j) J(r)\mathrm{d}r = 0, \quad j = +, -. \tag{66}$$

- The local constraint requiring the validity of the differential form of Gauss law $\varepsilon\varepsilon_0 \nabla \cdot \mathbf{E} = \rho\ (r)$, where $\rho(r) = e_0 \sum_{j=+,-} Z_j n_j(r)$ is the volume charge density:

$$\varepsilon\varepsilon_0 \frac{1}{r^\alpha}\frac{\partial(r^\alpha E(r))}{\partial r} - e_0 \sum_{j=+,-} Z_j n_j(r) = 0, \tag{67}$$

where in the planar geometry $\alpha = 0$, in the spherical geometry $\alpha = 2$, and in the cylindrical geometry $\alpha = 1$, while Z_j is the valency of the counter-ions ($j = +$) and coions ($j = -$).

The method of undetermined multipliers [34,58,57] is used to find the extreme of the free energy (63) taking into account the constraints (66) and (67). The described variational problem can be expressed by the Euler–Lagrange equations:

$$\frac{\partial L^*}{\partial E} - \frac{\mathrm{d}}{\mathrm{d}r}\left(\frac{\partial L^*}{\partial\left(\frac{\partial E}{\partial r}\right)}\right) = 0, \tag{68}$$

$$\frac{\partial L^*}{\partial n_j} = 0, j = +, - \tag{69}$$

where

$$L^*\left(E(r), n_+(r), n_-(r), \frac{\partial E(r)}{\partial r}, \eta(r)\right)$$
$$= J(r)\left[f\left(E(r), n_+(r), n-(r)\right) + \sum_{j=+,-}\lambda_j\left(n_j(r) - \Lambda_j\right)\right.$$
$$\left. -\eta(r)\left(\varepsilon\varepsilon_0\frac{1}{r^\alpha}\frac{\partial\left(r^\alpha E(r)\right)}{\partial r} - e_0\sum_{j=+,-}Z_j n_j(r)\right)\right], \tag{70}$$

λ_j, $j = +, -$, are the global Lagrange multipliers while $\eta(r)$ is the local Lagrange multiplier. Eqs. (68), (69) and (70) give

$$\eta(r) = \Phi(r) \tag{71}$$

$$kT\ln\frac{n_j n_{w0}}{n_0(n_s - \sum_i n_i)} + \lambda_j + e_0 Z_j\Phi(r) = 0. \tag{72}$$

From Eqs. (71), (72), and (39) the particle distribution functions are obtained [34,35]:

$$n_j(r) = \frac{n_s(n_0/n_{w0})\exp\left(-Z_j e_0\Phi(r)/kT\right)}{1 + (2n_0/n_{w0})\cosh\left(Z_j e_0\Phi(r)/kT\right)}, \tag{73}$$

where n_{w0} is the bulk concentration of *lattice sites occupied by water* molecules (see Eq. (39)):

$$n_{w0} = n_s - 2n_0. \tag{74}$$

It can be seen from Eq. (73) that close to the charged plane there may be a considerable excluded volume effect on the density profile of the counter-ions and on the solvent molecules. The concentration of the counter-ions is there comparable to the concentration of the solvent lattice sites so that the concentration of the solvent lattice sites deviates significantly from its value far from the charged surface [34]. Equation (73) also predicts a Fermi-Dirac-like distribution for counter-ions if the lattice constant a is large enough (see also Fig. 8). For higher values of surface charge density ($|\sigma|$) the counter-ion density saturates close to the charged surface to its close packing value, while the usual Poisson–Bolzmann theory predicts unreasonable high values beyond the close-packing value (see also [34,35,57]).

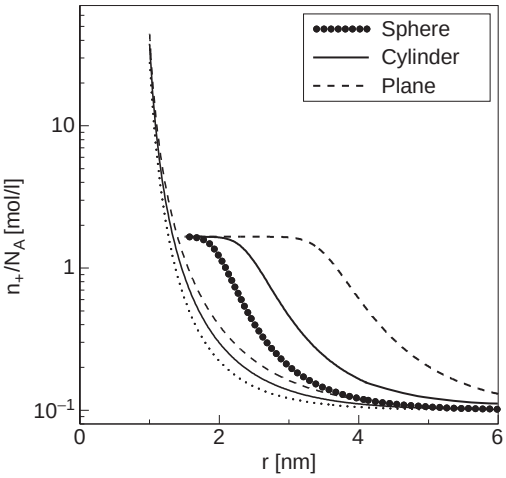

Figure 8 The concentration of counter-ions as a function of the distance from the charged surface. The results for the planar, cylindrical and spherical geometries are presented. The bold curves present results for the lattice constant of $a = 1$ nm, while the normal lines present the dimensionless ions. The model parameters are $\varepsilon = 78.5$, $T = 310$ K, $n_0/N_A = 0.1$ mol/l, $r_0 = 1$ nm and $|\sigma| = 0.4$ As/m^2[59], where N_A is Avogadro number.

The Gauss's law (Eq. (67)) and the particle distribution functions (Eq. (73)) give the differential equation for the electrostatic potential $\Phi(r)$:

$$\frac{d^2\Phi(r)}{dr^2} + \frac{\alpha}{r}\frac{d\Phi(r)}{dr} = \frac{2e_0 n_s n_0 Z}{\varepsilon\varepsilon_0 n_{w0}} \times \frac{\sinh\left(Ze_0\Phi(r)/kT\right)}{1 + (2_{n0}/n_{w0})\cosh\left(Ze_0\Phi(r)/kT\right)}, \quad (75)$$

where we take that $Z = |Z_+| = |Z_-|$.

The first boundary condition states that the electric field is zero far away from the charged surface:

$$\left.\frac{d\Phi(r)}{dr}\right|_{r=R} = 0, \quad (76)$$

where $R \to \infty$. The second boundary condition at the charged surface demands the electro-neutrality of the whole system:

$$\left.\frac{d\Phi(r)}{dr}\right|_{r=r_0} = -\frac{\sigma}{\varepsilon\varepsilon_0}. \quad (77)$$

In the limit of very dilute solution everywhere in the system: $\sum_{j=+,-} n_j(r) << n_w(r)$, and by taking into account the approximation $n_{w0} \simeq n_s$, where n_w (r) is the concentration of lattice sites occupied by water (solvent) molecules, the second term in the denominator of Eq. (75) can be neglected. Equation (75) then becomes:

$$\frac{d^2\Psi(r)}{dr^2} + \frac{\alpha}{r}\frac{d\Psi(r)}{dr} = \frac{\kappa^2}{Z}\sinh\Big(Z\Psi(r)\Big), \tag{78}$$

which is the well known PB equation (valid in the limit of dimensionless ions: $a \to 0$). We introduced the reduced electrostatic potential

$$\Psi = e_0\Phi/kT \tag{79}$$

and the Debye length

$$l_D = \kappa^{-1} = \sqrt{\frac{\varepsilon\varepsilon_0 kT}{2n_0 Z^2 e_0^2}}. \tag{80}$$

Neglecting the second term in denominator of Eq. (73) the particle distribution function (73) transforms into to the well known Boltzmann distribution function

$$n_j(r) = n_0 \exp\left(-Z_j\Psi(r)\right) \tag{81}$$

For illustration, Fig. 8 shows the concentration n_+ as a function of the distance r from the charged surface. The results are given for three different geometries: planar, cylindrical and spherical. The results of the Poisson–Boltzmann theory and the results of the functional density theory modified by the excluded volume effect with the lattice constant $a = 1$ nm are presented. In the planar geometry the excess of counter-ion concentration (calculated relative to its value far from the charged surface) protrudes deeper in the solution than in the cylindrical case, while in the cylindrical geometry the excess of the concentration distribution protrudes deeper into the solution than in the spherical geometry. The effect is more pronounced for larger ions. In all three geometries the saturation of the counter-ions near the charged surface (i.e. the Fermi-Dirac-like shape of distributions) for ions of finite size is obtained. The saturation value of the concentration of counter-ions is the same for all three geometries.

Figure 9 shows the electric potential dependence on the distance from the charged surface. The results for three different geometries are shown. The electric potential for the cylindrical geometry is smaller than the electric potential for the planar geometry whereas the electric potential for the cylindrical geometry is greater than the electric potential for the spherical geometry. Far from the charged surface the electric potential is insensitive to the geometry and to the lattice constant. The electric potential is higher for ions of finite size than for dimensionless ions.

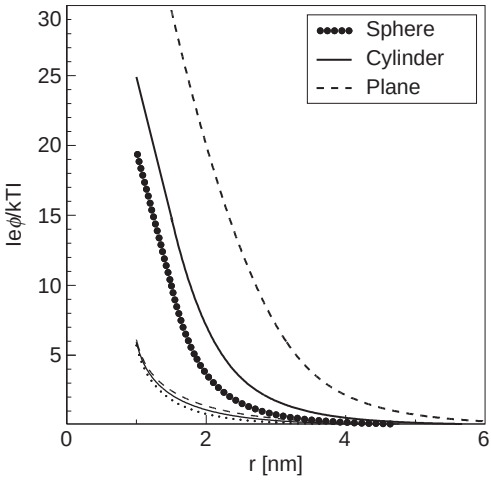

Figure 9 The electric potential as a function of the distance from the charged surface. The results for the planar, cylindrical and spherical geometries are presented. The bold curves present results for the lattice constant $a = 1$ nm, while the normal lines present the dimensionless ions. The model parameters are $\varepsilon = 78.5$, $T = 310$ K, $n_0/N_A = 0.1$ mol/l, $r_0 = 1$ nm, and $|\sigma| = 0.4$ As/m^2[59].

The ratio between the concentration of the counter-ions near the charged planar, cylindrical and spherical surfaces and the bulk counter-ion concentration in dependence on the surface charge density σ is presented in Fig. 10. This ratio is higher for dimensionless ions than for the ions of finite size. The discrepancy between the results for dimensionless ions and for the ions of finite size grows with increasing $|\sigma|$. The deviation can be attributed to steric effect of counter-ions and solvent molecules in a small region in the vicinity of the charged surface. The counter-ion concentration profile shows a rapid decrease for small lattice constant and a plateau region near the charged plane for large lattice constant. For large counter-ions we can therefore distinguish between two regions within the electric double layer: the saturated layer dominated by the steric repulsion and the diffuse layer extending into the solution.

3. Linearized Poisson–Boltzmann Theory

We consider a linear regime of Poisson–Boltzmann (PB) equation for monovalent ions ($Z = 1$), i.e., we assume that the electrostatic potential energy of an ion is much smaller than its thermal energy ($\Psi \ll 1$). We linearize sinh ($Z\Psi(r)$) in Eq. (78) and get:

$$\frac{d^2\Psi(r)}{dr^2} + \frac{\alpha}{r}\frac{d\Psi(r)}{dr} = \kappa^2\Psi(r) \tag{82}$$

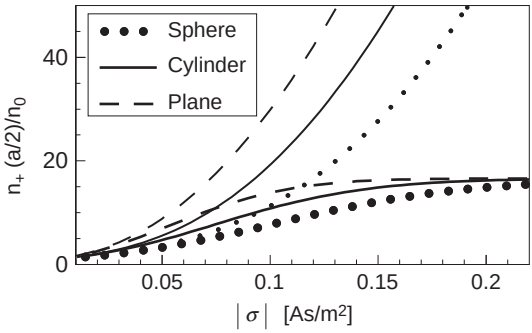

Figure 10 The ratio between the concentration of monovalent counterions near the charged planar, cylindrical, and spherical surfaces and the bulk counter-ion concentration in dependence on $|\sigma|$ [60]. The bold curves represent calculation for lattice constant 0.8 nm. The result of the Poisson–Boltzmann theory is given by the light curves. The model parameters are $\varepsilon = 78.5$, $T = 310$ K and $r_0 = 1$ nm.

3.1. Planar Geometry

In planar geometry ($\alpha = 0$), the Eq. (82) reduces to

$$\frac{\mathrm{d}^2\Psi(r)}{\mathrm{d}r^2} = \kappa^2\Psi(r). \tag{83}$$

By taking into account the boundary conditions (76) and (77) the solution of Eq. (83) for $r_0 = 0$ is

$$\Psi(r) = \Psi_0 e^{-\kappa r}, \tag{84}$$

where

$$\Psi_0 = 4\pi\sigma l_\mathrm{B} l_\mathrm{D}/e_0 \tag{85}$$

is the electrostatic potential near the charge surface and

$$l_\mathrm{B} = \frac{e_0^2}{4\pi\varepsilon\varepsilon_0 kT}. \tag{86}$$

is the Bjerrum length. Note that the electrostatic potential is proportional to the surface charge density. The electrostatic potential exponentially decreases with increasing distance from the charged surface. The thickness of the electric double layer is given by the Debye length $l_\mathrm{D} = 1/\kappa$ (see Eq. (80)).

3.2. Cylindrical Geometry

We consider a charged tube in contact with a solution of a symmetric monovalent solution of counter-ions and coions. The electric double layer inside the tube (concave case, Fig. 5) and outside the tube (convex case, Fig. 4) is considered.

In cylindrical geometry, $\alpha = 1$. Multiplying Eq. (82) by r^2 we get

$$r^2 \frac{\mathrm{d}^2\Psi(r)}{\mathrm{d}r^2} + r\frac{\mathrm{d}\Psi(r)}{\mathrm{d}r} - \kappa^2 r^2 \Psi(r) = 0. \tag{87}$$

The solution of differential Eq. (87) is [55]:

$$\Psi(r) = B_1 I_0(\kappa r) + B_2 K_0(\kappa r), \tag{88}$$

where I_0 is the modified Bessel function of first kind and 0-th order, while K_0 is the modified Bessel function of second kind and 0-th order. The constants B_1 and B_2 are determined from the boundary conditions.

In the case of the **concave** cylindrical electric double layer, the inner surface of the charged tube is in contact with the inner electrolyte solution. The boundary condition for the reduced potential $\Psi(r)$ inside the tube at the geometrical axis of the tube is

$$\left.\frac{\mathrm{d}\Psi(r)}{\mathrm{d}r}\right|_{r=0} = 0, \tag{89}$$

while the boundary condition at the inner charged surface of the tube is:

$$\left.\frac{\mathrm{d}\Psi(r)}{\mathrm{d}r}\right|_{r=R_\mathrm{i}} = \frac{\sigma_\mathrm{i} e_0}{\varepsilon\varepsilon_0 kT}, \tag{90}$$

where σ_i is the surface charge density of the inner surface of the tube, and R_i is the radius of the curvature of the inner charged surface of the tube (concave case). The boundary condition (90) reflects the electro-neutrality of the inner surface of the charged tube and the solution inside the tube

$$\int \rho_\mathrm{i} \mathrm{d}V + \oint \sigma_\mathrm{i} \mathrm{d}A = 0, \tag{91}$$

where ρ_i is the volume charge density of the inner solution. The first integral in Eq. (91) represents the total charge of the solution inside the tube, while the second integral represents the charge of the inner surface of the tube. Taking into account the Poisson Eq. (1)

$$\nabla^2\Psi = \frac{-4\pi l_\mathrm{B}\rho_\mathrm{i}}{e_0} \tag{92}$$

and the Gauss theorem, Eq. (91) transforms into the boundary condition (90). The first boundary condition (Eq. (89)) gives $B_2 = 0$, while from the second boundary condition (Eq. 90) the constant B_1 is determined. Inserting the constants B_1 and B_2 into Eq. (88) we obtain the electrostatic potential inside the tube:

$$\Psi(r) = \frac{\sigma_i e_0}{kT\varepsilon\varepsilon_0\kappa_i}\frac{I_0(\kappa_i r)}{I_1(\kappa_i R_i)}, \tag{93}$$

where I_1 is the modified Bessel function of the 1-st kind and $1/k_i$ is Debye length inside the tube:

$$1/\kappa_i = \sqrt{\frac{\varepsilon\varepsilon_0 kT}{2e_0^2 n_0^i}}. \tag{94}$$

The concentration of counter-ions inside the tube is given by the Boltzmann distribution

$$n_+^i = n_0^i e^{-\Psi(r)}, \tag{95}$$

where n_0^i is the bulk concentration of counter-ions and coions (the bulk solution often provides a suitable reference for the potential, see also [61]). In the linearized Poisson–Boltzmann theory the exponent in Eq. (95) can be expanded up to first order:

$$n_+^i = n_0^i(1 - \Psi(r)). \tag{96}$$

Inserting Eq. (93) into Eq. (96) we obtain

$$n_+^i = n_0^i\left(1 - \sigma_i\frac{4\pi l_B}{e_0\kappa_i}\frac{I_0(\kappa_i r)}{I_1(\kappa_i R_i)}\right), \tag{97}$$

where l_B is the Bjerrum length (see Eq. (86) for definition).

In the case of **convex** cylindrical electric double layer the outer surface of the charged tube is in contact with the outer solution of counter-ion and coions. The boundary condition for the reduced potential Ψ (r) outside the tube is

$$\left.\frac{d\Psi(r)}{dr}\right|_{r=R} = 0, \tag{98}$$

where $R \to \infty$. The boundary condition at the outer charged surface of the tube is

$$\left.\frac{d\Psi(r)}{dr}\right|_{r=R_o} = -\frac{\sigma_o e_0}{\varepsilon\varepsilon_0 kT} \tag{99}$$

where σ_o is the surface charge density of the outer surface of the tube and R_o is the radius of curvature of the outer charged surface of the tube (convex case). Taking into account the boundary conditions (98) and (99) the solution of Eq. (87) for the electrostatic potential $\Psi(r)$ is [61]

$$\Psi(r) = \frac{\sigma_o e_0}{kT\varepsilon\varepsilon_0\kappa_o}\frac{K_0(\kappa_o r)}{K_1(\kappa_o R_o)}. \tag{100}$$

The corresponding approximative expression (in linearized PB theory) for the concentration of counter-ions outside the charged tube is

$$n_+^o = n_0^o\left(1 - \sigma_o\frac{4\pi l_B}{e_0\kappa_o}\frac{K_0(\kappa_o r)}{K_1(\kappa_o R_o)}\right), \tag{101}$$

where K_1 is the modified Bessel function of the second kind and first order, $1/\kappa_o$ is Debye length outside the tube:

$$1/\kappa_o = \sqrt{\frac{\varepsilon\varepsilon_0 kT}{2e_0^2 n_0^o}} \tag{102}$$

and n_0^o is the concentration of counter-ions and coions far from the charged surface ($R \to \infty$), where the effect of the charged surface is negligible.

Similarly as in the concave case, the boundary condition (99) in the convex case reflects the electroneutrality of the outer surface of the charged tube and the solution of counter-ions and coions outside the tube:

$$\int \rho_o \mathrm{d}V + \oint \sigma_o \mathrm{d}A = 0, \tag{103}$$

where ρ_o is the volume charge density of the outer solution. The first integral in Eq. (103) represents the charge of the solution outside the tube, while the second integral represents the charge of the outer surface of the tube. Here we took into account the electro-neutrality of the outer surface of the charged tube and the solution outside the tube.

3.3. Spherical Geometry, Convex Case

In spherical geometry ($\alpha = 2$) and Eq. (82) reduces to

$$\frac{\mathrm{d}^2\Psi(r)}{\mathrm{d}r^2} + \frac{2}{r}\frac{\mathrm{d}\Psi(r)}{\mathrm{d}r} = \kappa^2\Psi(r). \tag{104}$$

The ansatz for the solution of this differential equation is

$$\Psi(r) = B_1\frac{e^{-\kappa r}}{r} + B_2\frac{e^{\kappa r}}{r} \tag{105}$$

In the case of charged spherical surface being on the outer side in contact with a solution of counter-ions and coions (convex case) the coefficients B_1 and B_2 are determined from the boundary conditions (see Eqs. (76) and (77)):

$$\left.\frac{d\Psi(r)}{dr}\right|_{r=R} = 0, \tag{106}$$

$$\left.\frac{d\Psi(r)}{dr}\right|_{r=r_0} = -\frac{\sigma e_0}{\varepsilon\varepsilon_0 kT}. \tag{107}$$

The boundary condition (106) demands that the electric field far from the charged spherical surface ($R\to\infty$) is zero and determines $B_2 = 0$. The boundary condition (107) at the charged surface yields

$$B_1 = \frac{r_0^2 e^{\kappa r_0}}{1+\kappa r_0}\cdot\frac{\sigma l_B 4\pi}{e_0} \tag{108}$$

The final solution of Eq. (104) is thus given by

$$\Psi(r) = \Psi_0 \frac{r_0}{r} e^{\kappa(r_0-r)} \tag{109}$$

where

$$\Psi_0 = \frac{r_0}{1+\kappa r_0}\times\frac{\sigma l_B 4\pi}{e_0} \tag{110}$$

4. Thickness of Electric Double Layer

In this section the thickness of a single electric double layer is considered. The screening of the electrostatic field by the counter-ions that accumulate near the charged plane can be represented by the effective thickness of the electric double layer. The thickness of electric double layer measures the range of the electrostatic influence of the charged surface in the surroundings. In the planar geometry we introduce the distance x_ϑ where the concentration of the counter-ions (calculated relative to its value far from the charged surface) drops to a fraction $(1-\vartheta)$ of the value of $n_+(a/2)$ [59]

$$n_+(x_\vartheta) - n_0 = (1-\vartheta)(n_+(a/2) - n_0), \tag{111}$$

where $\frac{a}{2}$ is the distance of the closest approach.

We introduce another measure of the thickness of the electric double layer, namely the distance d_ϑ, defining the region that contains a certain fraction ϑ of the excess of the counter-ions [59]

$$\int_{a/2}^{d_\vartheta}(n_+(x)-n_0)\mathrm{d}x=\vartheta\int_{a/2}^{d}(n_+(x)-n_0)\mathrm{d}x \tag{112}$$

For vanishing ion size (in the limit of the validity of the Poisson–Boltzmann theory) x_ϑ is expressed analytically:

$$x_\vartheta=\frac{1}{\kappa}\ln\left(\frac{\left(\sqrt{(1+(1-\vartheta)\left(\exp\left(\frac{-Z_+e_0\Phi(0)}{kT}\right)-1\right)}+1\right)\left(1-\exp\left(\frac{Z_+e_0\Phi(0)}{2kT}\right)\right)}{\left(\sqrt{(1+(1-\vartheta)\left(\exp\left(\frac{-Z_+e_0\Phi(0)}{kT}\right)-1\right)}-1\right)\left(1+\exp\left(\frac{Z_+e_0\Phi(0)}{2kT}\right)\right)}\right), \tag{113}$$

where

$$\Phi(0)=-\frac{2kT}{Z_+e_0}\ln\left(\sqrt{1+(\sigma/c)^2}+|\sigma|/c\right) \tag{114}$$

and

$$c=\sqrt{8kT\varepsilon\varepsilon_0 n_0}. \tag{115}$$

Subject to the same limit, and taking that $R\to\infty$, the parameter d_θ may be expressed as

$$d_\vartheta=\frac{1}{\kappa}\ln\left(\frac{1+\frac{1+\vartheta}{1-\vartheta}\exp\left(\frac{Z+e_0\Phi(0)}{2kT}\right)}{\left(1+\exp\left(\frac{Z+e_0\Phi(0)}{2kT}\right)\right)}\right). \tag{116}$$

If, in addition, $|e_0\,\Phi(x)/kT| \ll 1$ for all x, i.e., the linearized Poisson–Boltzmann theory is applied, both measures further simplify into the expression

$$x_\vartheta=d_\vartheta=\frac{1}{\kappa}\ln\frac{1}{1-\vartheta}, \tag{117}$$

where $1/\kappa$ is the Debye screening length (see Eq. (80)), which describes the effective thickness of the electric double layer in the linearized Poisson–Boltzmann theory.

Figure 11 shows the parameters x_ϑ (representing the effective thickness of the electric double layer) in dependence of the lattice size a that represents the ion size for three choices of ϑ: 0.9, 0.8, and 0.5. The points marked by the dots show the results of the Poisson–Boltzmann theory. The values of the parameters x_ϑ are larger for higher ϑ, however, qualitative dependence is equal for all three choices. For small values of ϑ both parameters diminish while as ϑ approches 1, both parameters increase beyond every bound. We see that the effective thickness of the electric

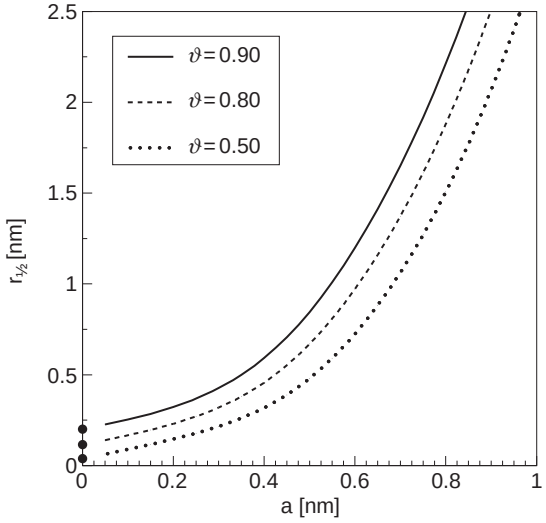

Figure 11 Thickness $r_{1/2}$ of the planar electric double layer as a function of the lattice constant a [59]. The point denotes the corresponding results of the nonlinearized PB theory. The model parameters are $\varepsilon = 78.5$, $T = 310$ K, $n_0/N_A = 0.1$ mol/l and $|\sigma| = 0.4$ As/m^2.

double layer increases with increasing size of the counter-ions, reaching the values of several nanometers for lattice constants of about 1 nanometer. The limit of small lattice constant a corresponds well with the Poisson–Boltzmann theory.

The parameter ϑ should not be too low as for small ϑ only a small part of the excess of the counter-ions is involved in the region $x < x_\vartheta$. On the other hand, for ϑ very close to 1 the thickness of electric double layer is almost independent of all the parameters as the region must contain almost all the excess counter-ions. It is sensible to choose ϑ somewhere between 0.4 and 0.8 where the effect of different other parameters is clearly exhibited.

The thickness of the electric double layer in cylindrical geometry (see. Fig. 12 is described by the characteristic length $r_{1/2}$, i.e., the distance from the charged surface where the excess of the counter-ions drops to a half of its value near the distance of closest approach to the charged cylindrical surface. Within the presented theory where the excluded volume effect is taken into account, the thickness of the diffuse layer $r_{1/2}$ is always larger than within the PB theory. When finite size of ions is considered, the shielding of the electric field of the charged surface is less effective than in the PB theory where there is no limit regarding to the concentration of counter-ions. For small parameters $\xi = \sigma\, r_0 e_0/2\varepsilon\varepsilon_0 kT$ the effective thickness of the electric double layer is decreasing with increasing ξ as the surface bearing higher charge attracts in its vicinity larger number of counter-ions. Consequently the screening is more effective. If we further increases the parameter ξ, the influence of the excluded volume effect increases with increasing ξ. The effective thickness $r_{1/2}$ after reaching its minimum, begins to increase with increasing ξ. This is the result of the fact that the excluded volume imposes an upper limit on the

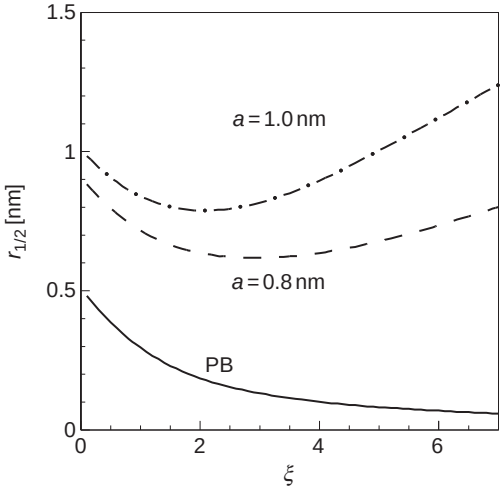

Figure 12 Thickness r_ϑ of the cylindrical electric double layer as a function of the linear charge parameter ξ for two different lattice constants a [59]. The results of PB theory is also shown. The model parameters are $\varepsilon = 78.5$, $T = 310$ K, $n_0/N_A = 0.1$ mol/1 and $r_0 = 1$ nm.

concentration of counter-ions. There is no upper limit of the concentration of ions in the PB theory and the effective thickness in the PB theory decreases monotonously with ξ. No minimum is reached.

5. Effect of Intra-Ionic Correlations on the Interaction between Two Electric Double Layers

First we consider an aqueous electrolyte solution sandwiched between two large, planar equally charged surfaces. Each surface is carrying a uniform average negative surface charge density $\sigma = -e_0/a$ where e_0 is the elementary charge and a is the average cross-sectional area per charge on the surface. The distance between the two surfaces is D. The electrostatic field varies only in the normal direction between charged surfaces (x-direction). We assume that there is no electric field behind the charged plates. The solution is composed of rod-like quadrupolar (divalent) ions with charge spatially distributed within the ion (see also Fig. 13).

5.1. A System of Two Interacting Double Layers Composed of Point-like Ions

We consider a system of two parallel like-charged planar surfaces immersed in the solution of point-like counter-ions and coions. Electrostatic free energy of the system is composed of the electrostatic energy and the entropic contribution to the free energy (see Eqs. (3) and (33)) [34,62]:

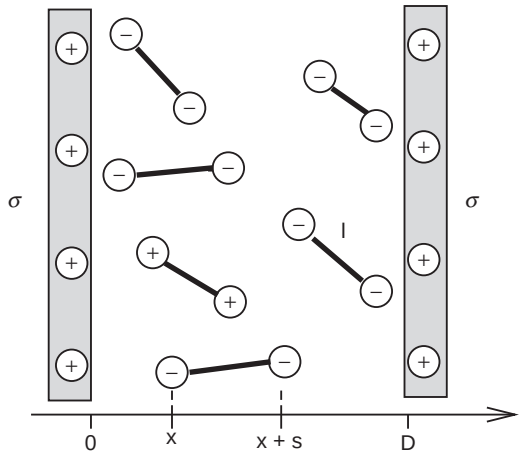

Figure 13 Schematic illustration of two like-charged planar surfaces, located at $x = 0$ and $x = D$ with σ denoting the corresponding surface charge density. The surfaces are immersed in an electrolyte solution that contains negatively and positively charged rod-like divalent counter-ions and coions. The separation between the individual charges of each rod-like ion is denoted by l. The coordinates x and $x + s$ specify the instantaneous positions of the two charges in a given rod-like ion along the horizontal axis [5].

$$\frac{F}{AkT} = \frac{1}{8\pi l_B}\int_0^D \Psi'^2 dx + \int_0^D \left[n_+ \ln \frac{n_+}{n_0} + n_- \ln \frac{n_-}{n_0} - (n_+ + n_- - 2n_0)\right] dx, \tag{118}$$

where Ψ is the reduced electrostatic potential (see Eq. (79)), $n_+(x)$ is the concentration of counter-ions, $n_-(x)$ is the concentration of coions, and n_0 is the bulk concentration of counter-ions and coions. The first variation of the electrostatic free energy (Eq. 118) takes the form:

$$\frac{\delta F}{AkT} = \int_0^D dx \left\{ \delta n_+ \left[Z\Psi + \ln \frac{n_+}{n_0} \right] + \delta n_- \left[-Z\Psi + \ln \frac{n_-}{n_0} \right] \right\}, \tag{119}$$

where Z is the valency of counter-ions and coions. The variation δF depends only on the variations of n_+ and δn_-. Here the variation of the Ψ'^2 in F was performed by taking into account the relation $\Psi'\delta\Psi' = (\Psi\delta\Psi')' - \Psi\delta\Psi''$ and

$$\delta''\Psi = -4\pi l_B \frac{\delta\rho}{e_0}, \tag{120}$$

where the volume charge density is given by $\rho = Ze_0 (n_+ - n_-)$. In the thermodynamic equilibrium the electrostatic free energy has to be minimal with respect to n_+ and n_-. Therefore we have to fulfill the condition:

$$\delta F = 0. \tag{121}$$

The result of the variational procedure gives the concentration profiles:

$$n_+ = n_0 e^{-Z\Psi}, \tag{122}$$

$$n_- = n_0 e^{Z\Psi}. \tag{123}$$

Inserting Eqs. (122) and (123) into the Poisson equation gives the following differential equation:

$$\psi'' = \frac{2Ze_0^2 n_0}{\varepsilon\varepsilon_0 kT} \sinh(Z\Psi). \tag{124}$$

The boundary conditions are given at the charged surfaces:

$$\frac{\mathrm{d}\Psi}{\mathrm{d}x}(x=0) = -\frac{4\pi l_B \sigma}{e_0}, \tag{125}$$

and

$$\frac{\mathrm{d}\Psi}{\mathrm{d}x}(x=D) = \frac{4\pi l_B \sigma}{e_0}, \tag{126}$$

which are equivalent to the overall electroneutrality of the system.

The equilibrium free energy of the system is obtained by inserting the concentration profiles (122) and (123) into the Eq. (118)

$$\frac{F}{AkT} = \frac{1}{8\pi l_B}\int_0^D \left[\psi'^2 + \frac{2\Psi}{Z}\sinh(Z\Psi) - \frac{2}{Z^2}\cosh(Z\Psi) + \frac{2}{Z^2}\right]\mathrm{d}x. \tag{127}$$

The electrostatic free energy depends on the distance between the charged surfaces, the surface charge density and the valency Z. The PB theory for divalent point-like ions always gives a repulsive interaction between equally charged surfaces.

5.2. Rod-like Quadrupolar (Divalent) Nanoparticles

We consider a system of two parallel charged surfaces immersed in the solution of multivalent rod-like counter-ions and coions (Fig. 13). In our model the rod-like ions are composed of two individual charges of valency Z separated by a fixed distance l. The rod-like counter-ions are characterized by positional and orientational degrees of freedom. We describe them by referring to one of the two charges of each particle as a reference charge, denoting the local concentration of all the reference charges by $n_i(x)$. The location of the second charge of a given counter-ion will be specified by the conditional probability distribution $p_i(s|x)$, denoting the

probability to find the second charge at position $x + s$ if the first is at x. At any given position x, we require the normalization condition $\frac{1}{2l}\int_{-l}^{l} \mathrm{d}s\ p_i(s|x) = 1$ to be fulfilled. Note also that $p_i\,(s|x) = 0$ for $|s| > l$.

The free energy of the system, measured per unit area of the surface and divided by unit of energy kT, consists of three terms: electrostatic energy (Eq. (3)), configurational entropy (Eq. (33)) and orientational entropy of the multivalent rod-like particles [5]

$$\begin{aligned}\frac{F}{AkT} = \frac{1}{8\pi l_{\mathrm{B}}}\int_0^D \mathrm{d}x\boldsymbol{\Psi}'(x)^2 \\ + \sum_{i=\{+,-\}} \int_0^D \mathrm{d}x\left[n_i(x)\ \ln\ \left[\frac{n_i(x)}{n_0}\right] - \Big(n_i(x) - n_0\Big)\right] \\ + \sum_{i=\{+,-\}} \int_0^D \mathrm{d}x\ n_i(x)\frac{1}{2l}\int_{-l}^{l} \mathrm{d}s\ p_i(s|x)[\ \ln\ p_i(s|x) + U(x,s)],\end{aligned} \tag{128}$$

where $\boldsymbol{\Psi}$ is the reduced electrostatic potential (see Eq. (79)), l_{B} is the Bjerrum length (see Eq. (86) for definition), and n_0 is bulk value of ion concentration. We introduce a function:

$$U(x,s) = \begin{cases} 0, x > 0 \text{ and } x + s > 0 \text{ and } x > D \text{ and } D - x - s > 0 \\ \infty, \text{elsewhere} \end{cases}$$

which takes into account that integration over ds for the rod-like counter-ions near the boundaries can not be held over the whole integration range from $-l$ to l if the distance between the reference charge and the charged surface is less than l. In thermal equilibrium, the free energy $F = F[n_i\,(x), p_i\,(s|x)]$ is minimal with respect to $n_i\,(x)$ and $p_i\,(s|x)$. The results of variation ($\delta F = 0$) gives the normalized conditional probability density

$$p_i(s|x) = \frac{e^{-U(x,s) - Zi\boldsymbol{\Psi}(x+s)}}{(1/2l)\int_{-l}^{l} \mathrm{d}\,\bar{s}\, e^{-U(x,\bar{s}) - Zi\boldsymbol{\Psi}(x+\bar{s})}} \tag{129}$$

and the local concentration of reference charges $n_i\,(x)$ of multivalent rod-like ions

$$n_i(x) = n_0 e^{-Zi\boldsymbol{\Psi}(x)}\frac{1}{2l}\int_{-l}^{l} \mathrm{d}s\ e^{-U(x,s) - Zi\ \boldsymbol{\Psi}(x+s)} \tag{130}$$

The volume charge density

$$\frac{\rho(x)}{e_0} = \sum_{i=\{+,-\}}\left[Zn_i(x) + Z\frac{1}{2l}\int_{-l}^{l} \mathrm{d}s\ n_i(x-s)\ p_i(s|x-s)\right]. \tag{131}$$

includes contributions from a reference charge located at x and from a second, orientationally mobile charge located at $x - s$. If we insert the concentration n_i (x, s) (Eq. (130)) and the conditional probability density (Eq. (129)) into the volume charge density Eq. (131) and use the Poisson equation Ψ'' $(x) = -4\ \pi l_B\ \rho(x)/e_0$, we obtain the nonlinear integro-differential equation

$$2\Psi''(x) = \kappa^2 \frac{1}{2l} \int_{-\min(l,x)}^{\min(l,D-x)} \mathrm{d}s\ \sinh[\Psi(x) + \Psi(x+s)], \tag{132}$$

where $\kappa^2 = 4 \times 8\pi l_B n_0$. Integration limits are defined by the minimum or the maximum of the both values given in brackets. Equation (132) is valid in the region $0 \leq x \leq D$. The boundary conditions at the charged surfaces are:

$$\begin{aligned} \Psi'(x=0) &= -\frac{4\pi l_B \sigma}{e_0}, \\ \Psi'(x=D) &= -\frac{4\pi l_B \sigma}{e_0}. \end{aligned} \tag{133}$$

Fig. 14A shows the reduced electrostatic potential Ψ $(\bar{x})/p$ as a function of the distance $\bar{x}$ from the macroion. The length are scaled by the Debye length $l_D = 1/\kappa$. The dimensionless charge parameter is given by $p = 2\pi l_B l_D/a$. The different curves correspond to different rod length $\bar{l}$. Plotting $\Psi(\bar{x})/p$ is convenient because $\Psi(\bar{x})$ $\sim p$ in the linear regime. Clearly, for $\bar{l} = 0$ the potential agrees with the Poisson–Boltzmann theory for monovalent ions. Note that the potential increases more rapidly with decreasing x for non-vanishing $\bar{l}$ than for $\bar{l} = 0$. Upon increasing $\bar{l}$ beyond $\bar{l} > \bar{l}_c \approx 2$ the potential develops non-monotonic behavior. This behavior directly implies "overcharged" regions where the charges from the rod-like ions over-compensate the macroion charge density at a certain distance away from the macroion. This conclusion follows from the scaled integrated charge (charge per unit area) at distance $\bar{x}$,

$$Q(\bar{x}) = -\frac{l_D}{\sigma} \int_0^{\bar{x}} \rho(\bar{x}) \mathrm{d}\,\bar{x}, \tag{134}$$

which generally adopts the values $Q(0) = 0$ and $Q(\bar{D}/2) = 1$. In addition, $Q(\bar{x}) > 1$ signifies "overcharging." Rewriting $Q(\bar{x}) = 1 + \Psi'(\bar{x})/(2p)$ we see that regions with $\Psi'(\bar{x}) > 0$ imply $Q(\bar{x}) > 1$. The inset of Fig. 14A displays $Q(\bar{x})$ corroborating "overcharging" for $\bar{l} \gtrsim 2$. For $\bar{l} \gtrsim 2$ there is no critical charge parameter p at which the overcharging first appears.

Even though the potential $\Psi(\bar{x})$ in Fig. 14A is smooth, the corresponding ionic densities $n_{\pm}(\bar{x})$ are not. This can be seen for any $\bar{l} > 0$ directly in the limit of $p = 0$ where electrostatic interactions are not relevant any more; $\Psi \equiv 0$ and $n_+(\bar{x}) = n_-(\bar{x})$. The steric interactions of the rod-like ions still lead to a depletion from the macroions; for $\bar{D} > 2\bar{l}$ the densities are $n_{\pm}(\bar{x})/n_0 = (1 + \bar{x}/\bar{l})/2$ for $0 \leq \bar{x} \leq \bar{l}$

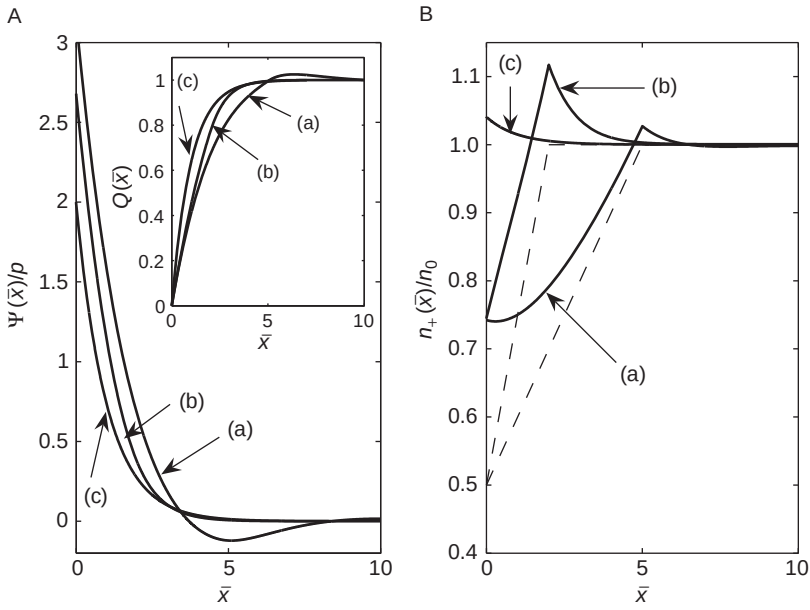

Figure 14 Results for the linearized theory, derived for large distance $\bar{D} = 20$ between the two surfaces [5]. (A) Electrostatic potential $\Psi(\bar{x})/p$ as a function of the distance $\bar{x}$ from the charged surface. The inset shows the scaled integrated charge according to Eq. (134). (B) Local concentration of reference charges $n_+(\bar{x})/n_0$ as a function of $\bar{x}$, derived for $p = 0.1$. Dashed lines display corresponding calculations where electrostatics is excluded ($p = 0$). In all diagrams the different curves correspond to $\bar{l} = 5$ (a), $\bar{l} = 2$ (b), and $\bar{l} = 0$ (c).

and $n_{\pm}(\bar{x})/n_0 = 1$ for $\bar{l} \leq \bar{x} \leq \bar{D}/2$. These functions are plotted in Fig. 14B (dashed curves, for different rod-lengths $\bar{l}$) together with the corresponding results (solid curves) for $n_+(\bar{x})$ in the presence of electrostatic interactions for $p = 0.1$. Again, different curves (a), (b), and (c) correspond to different rod lengths $\bar{l}$.

From known electrostatic potential $\Psi(\bar{x})$ the electrostatic free energy can be calculated. Fig. 15 shows the electrostatic free energy as a function of the distance between two equally charged surfaces. The free energy F is calculated in linear and in the nonlinear regime. Fig. 15 shows results for a characteristic case of long ions; $\bar{l} = 5$. We see that in the limit of $p = 0$ and for $\bar{D} > \bar{l}$, we find $F \times 16\pi l_B l_D/(AkT) = \bar{l}/2$, (or, equivalently, $F/(AkT) = ln_0$), indicating that the two flat surfaces no longer interact with each other. For small distances, $\bar{D} < \bar{l}$, there is entropy loss of the mobile rods due to their interaction with *both* surfaces occurs. The corresponding depletion attraction continues to dominate the system for weakly charged surfaces where $p \ll 1$, leading to a minimum in $F(\bar{D})$ at small $\bar{D} < \bar{l}$. For larger surface charge density, $p \gtrsim 1$, a depletion minimum is absent. A second minimum, located roughly at $\bar{D} \approx \bar{l}$, is weak for $p \ll 1$ but dominates the system for $p \gtrsim 1$. This second minimum is distinct from the depletion minimum; it is electrostatic in origin and can be ascribed to a *bridging mechanism* (Fig. 16). In support of this notion, the bridging minimum occurs for highly charged surfaces almost exactly at $\bar{D} = \bar{l}$; see curve (a) in Fig. 15. The linearized integro-differential

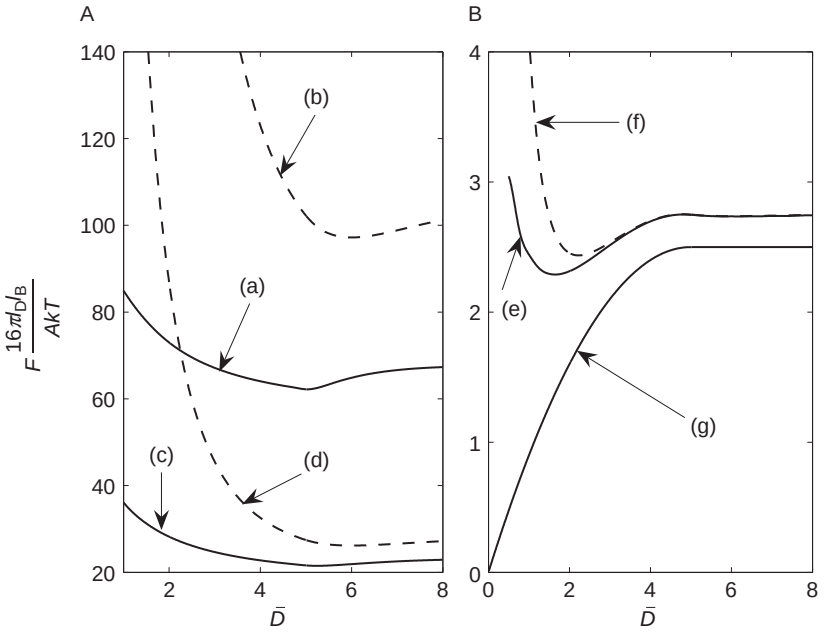

Figure 15 Scaled free energy F as a function of the distance between the two charged planar surfaces, $\bar{D}$, for $\bar{l} = 5$ [5]. In both diagrams, the solid curves are derived using nonlinear theory, while the dashed curves are based on linearized theory. The charge parameters correspond to $p = 2$ (a,b), $p = 1$ (c,d), and $p = 0.1$ (e,f). Finally, for curve (g) it is $p = 0$, and no electrostatic interactions are present.

equation (see the dashed curves in Fig. 15) yields qualitatively the same predictions as the full nonlinear theory (see the solid curves in Fig. 15). Yet, as for point-like mobile ions, the free energies of the former are much larger if $p \gtrsim 1$.

The theoretical studies of electric double layer of large rod-like quadrupolar (divalent) ions in contact with charged (membrane) planar surface [3,5] have motivated further theoretical studies of the physical properties of a solution of large multivalent ions in contact with a highly charged plane [7,63], such as a solution of large phosphotungstate charged nanoparticles (with diameter around 1 nm) in contact with a highly charged monolayer composed of eicosylamine [64]. The counter-ions were described as spheres with spatially distributed charge [7,63] (see also Fig. 1).

It was shown that at finite temperatures and high enough surface charge densities, the internal charge distribution within a single spherical multivalent charged nanoparticle (with the internal charges located at large enough distances l, see Fig. 1) may lead to the orientational ordering of these multivalent nanoparticles near a charged surface, where the main axis of the nanoparticles (which coincides with the line connecting the two poly-ions with charge $e/2$) is predominantly oriented perpendicularly to the charged surface [63].

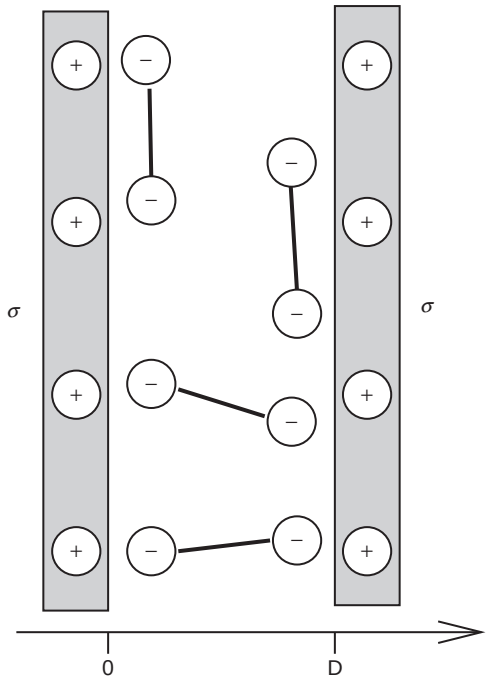

Figure 16 Schematic illustration of the bridging mechanism. For long rod-like ions, $T \gg 1$, there exists a stable equilibrium between the two charged surfaces at $D \approx T$. Here, the ions preferentially orient either parallel or normal to the macroion surfaces. Those aligning normal give rise to the bridging equilibrium [5].

Moreover, it was shown recently that the above described orientational ordering of spherical multivalent charged nanoparticles may give rise to an attractive interaction between like-charged membrane surfaces for high enough surface charge densities of the interacting surfaces and large enough separations between internal charges l [63]. In accordance, we also experimentally observed monoclonal antibody-mediated coalescence of negatively charged giant unilamellar phospholipid vesicles upon close approach of the vesicles [7].

5.3. Dipolar Rod-like Nanoparticles in Electrolyte Solution

Recently, small dipoles [65] and large dipolar rod-like nanoparticles [4] in electrolyte solution of monovalent ions between two oppositely charged planes have also been studied. In this section we describe only the second case (Fig. 17). The dipolar nanoparticles have internal structure, each dipole is composed of negative and positive elementary charges of valency Z, separated by a distance l, i.e., the dipole moment of each dipole is Ze_0l, where e_0 is the elementary charge. The dipoles are characterized by the positional and the orientational degrees of freedom while the monovalent ions are characterized only by the positional degree of freedom. We describe the dipole by referring to the positive charge as a reference charge, denoting the local concentration of all the reference charges by $n(x)$. The location of the

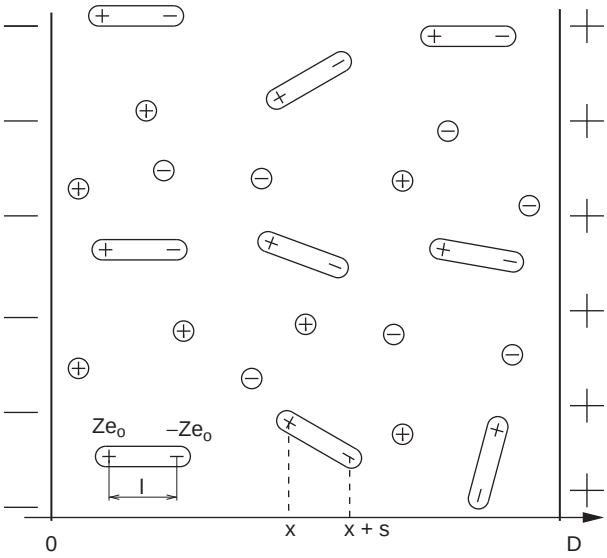

Figure 17 Schematic presentation of two oppositely charged planar surfaces, which is filled with water containing dipoles with dipole moment $Ze_0 l$ and monovalent positive and negative ions. The separation between the individual charges of each dipole is denoted by l. The valency of each charge of the dipole is Z.

negative charge of a given dipole is specified by the conditional probability density $p(s|x)$, denoting the probability to find the negative charge at position $x + s$ if the positive is at x. At any given position x, we require the normalization condition $\frac{1}{2l}\int_{-l}^{l} \mathrm{d}s p(s|x) = 1$ to be fulfilled. Note also that $p(s|x) = 0$ for $|s| > l$.

The free energy of the system per unit area of the surface A and thermal energy kT is composed of the energy stored in the electrostatic field (Eq. (3)), the configurational (Eq. (15)) and orientational entropy of the dipoles as well as the configurational entropy of the monovalent ions (Eq. (33)) [4]:

$$\begin{aligned}\frac{F}{AkT} = {} & \frac{1}{8\pi l_B}\int_0^D \mathrm{d}x\, \psi'(x)^2 + \int_0^D \mathrm{d}x[n(x)\ \ln\ \upsilon_0 n(x) - n(x)] \\ & + \int_0^D \mathrm{d}x\ n(x)\frac{1}{2l}\int_{-l}^{l} \mathrm{d}s\ p(s|x)[\ \ln\ p(s|x) + U(x,s)] \\ & + \int_0^D \mathrm{d}x\ n(x)\lambda(x)\left[\frac{1}{2l}\int_{-l}^{l} \mathrm{d}s\ p(s|x) - 1\right] \\ & + \mu\int_0^D \mathrm{d}x\left[n(x) - \frac{N}{AD}\right] \\ & + \int_0^D \mathrm{d}x \sum_{i=\{+,-\}}\left[n_i(x)\ \ln\ \frac{n_i(x)}{n_{0s}} - (n_i(x) - n_{0s})\right]\end{aligned} \tag{135}$$

where Ψ is the reduced electrostatic potential (see Eq. (79)), μ is global Lagrange multiplier, υ_0 is the volume of the dipole, l_B is the Bjerrum length (see Eq. (86) for definition), N is the number of dipoles, n_i is the concentration of the monovalent ions of the i-th type and n_{0s} is the bulk concentration of monovalent ions. The sum in Eq. (135) runs over positive "i = +" and negative "i = −" monovalent ions. The Lagrange parameter $\lambda(x)$ ensures the normalization condition for the conditional probability density. The fifth term in Eq. (135) ensures the constant number of dipoles in the solution. We introduce the external reduced potential of the charged wall

$$U(x,s) = \begin{cases} 0, & x > 0 \text{ and } x + s > 0 \text{ and } x < D \text{ and } D - x - s > 0 \\ \infty, & \text{elswhere} \end{cases}$$

which ensures that the dipoles could not penetrate into the charged wall.

In thermal equilibrium, the free energy $F = F[n(x), p(s|x), n_i(x)]$ is minimal with respect to the functions $n(x)$, $p(s|x)$ and $n_i(x)$. The variational procedure ($\delta F = 0$) gives the local concentration of monovalent ions

$$n_i(x) = n_{0s} e^{-i\Psi(x)}, \tag{136}$$

the conditional probability density

$$p(s|x) = \frac{e^{-U(x,s)+Z\Psi(x+s)}}{q(x)} \tag{137}$$

and the local concentration of reference charges of dipoles

$$n(x) = n_0 e^{-Z\Psi(x)} q(x) \tag{138}$$

where $n_0 = \frac{1}{\upsilon_0} e^{-\mu}$ is the concentration of reference charges at vanishing electrostatic ($\Psi = 0$) and external ($U = 0$) potentials, and

$$q(x) = \frac{1}{2l} \int_{-l}^{l} \mathrm{d}s \; e^{-U(x,s)+Z\,\Psi(x,s)} \tag{139}$$

is the orientational partition function of a single dipole with the position of its reference charge at x. In Eq. (138) the term $e^{-Z\,\Psi(x)}$ corresponds to the Boltzmann distribution of the reference charges of dipoles.

The local charge density includes contributions from positive reference charges that are located at x and from the orientational mobile negative charges, located at $x - s$ with the corresponding probability density $p(s|x - s)$ as well as from the positive and negative charges of monovalent ions. Inserting the local charge density

$$\frac{\rho(x)}{e_0} = Zn(x) - Z\frac{1}{2l}\int_{-l}^{l} \mathrm{d}s \; n(x-s)p(s|x-s) + \sum_{i=\{+,-\}} i n_i(x) \tag{140}$$

into the Poisson equation $\Psi''(x) = -4\pi l_B(\rho(x)/e_0)$ we obtain the integro-differential equation for the reduced electrostatic potential

$$\Psi''(x) = 8\pi l_B Z n_0 \frac{1}{2l}\int_{\max[-l,-x]}^{\min[l,D-x]} ds\, \sinh[Z\Psi(x) - Z\Psi(x+s)] + 8\pi l_B n_{0s} \sinh[\Psi(x)] \tag{141}$$

The boundary conditions are given at the charged plates:

$$\Psi'(x=0) = -\sigma\frac{4\pi l_B}{e_0} \tag{142}$$

$$\Psi'(x=D) = -\sigma\frac{4\pi l_B}{e_0} \tag{143}$$

These boundary conditions demand a neutral overall charge for the system.

In the case of the solution composed of only monovalent ions ($n_0 = 0$, the dipoles are not present) the integro-differential Eq. (141) reduces to the well known PB equation for the monovalent salt of ions $\Psi''(x) = 8\pi l_B n_{0s} \sinh[\Psi(x)]$.

If the electrostatic potential is small compared to the thermal energy ($\Psi \ll 1$), we can linearize the term $\sinh[Z\Psi(x) - Z\Psi(x+s)]$ in Eq. (141) to $Z\Psi(x) - Z\Psi(x+s)$ and the term $\sinh[\Psi(x)]$ to $\Psi(x)$. The linearized integro-differential equation is

$$\Psi''(x) = 8\pi l_B Z n_0 \frac{1}{2l}\int_{\max[-l,-x]}^{\min[l,D-x]} ds[Z\Psi(x) - Z\Psi(x+s)] + 8\pi l_B n_{0s}\Psi(x) \tag{144}$$

with the same boundary conditions (142) and (143).

Figure 18A shows the reduced electrostatic potential Ψ and the electric field strength E (in the inset) as a function of the distance from the left charged surface (x) for three different lengths of dipoles. The electrostatic potential Ψ monotonously increases with increasing distance from the left charged surface. The electric field strength E is symmetric with respect to the midplane of the system. In the limit of very small dipoles the electrostatic potential reduces to the electrostatic potential of the condenser filled with water and the electric field strength becomes constant $E_0 = -7.1 \cdot 10^6$ V/m. The difference between the field strength and the constant value E_0 increases with increasing length of dipoles.

Figure 18B shows the concentration of reference charges n while Figure 18C shows the charge density ρ as a function of the distance from the left charged plate (x) for three different lengths of dipoles. The concentration of reference charges n first increases, reaches maximum value and than decreases with increasing x. In the

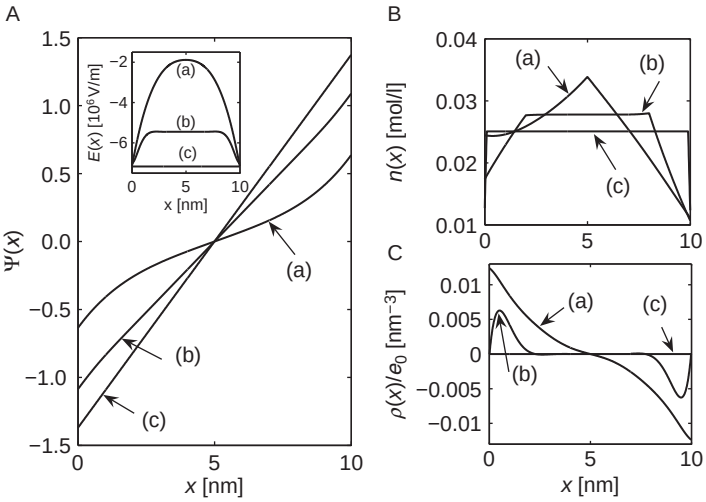

Figure 18 Linearized theory. Salt of monovalent ions is not present [4]. (A) Reduced electrostatic potential $\Psi(x)$ and electric field strength $E(x)$ (in inset), (B) local concentration of reference charges $n(x)$ and (C) charge density $\rho(x)$ as a function of the distance from the left charged plate x. The length of dipoles $l = 5$ nm (a), $l = 2$ nm (b) and $l = 0.1$ nm (c) are shown. The volume of dipole is $v_0 = la_0$. Model parameters are $D = 10$ nm, $a_0 = 1$ nm^2, $\sigma = 0.005$ As/m^2, $Z = 1$, $\varepsilon = 78$, $T = 300$ K and $N = 25$ for $A = 100$ nm^2.

limit $l = 0$ the concentration n reaches a constant value. The local concentration of reference charges $n(x)$ is not smooth (Fig. 18B). The first derivative of $n(x)$ is discontinuous at $x = l$ and $x = D - l$. In the regions $0 < x < l$ and $D - l < x < D$ the orientational restriction of dipoles is present. In the region $l < x < D - l$ the orientational restriction of dipoles is not present. For longer dipoles l the absolute value of the charge density ρ decreases with increasing distance from the left charged surface. For smaller l the absolute value of the charge density ρ first increases, reaches a maximum and then decreases with increasing distance to attain the zero value in the centre of the system. In the limit of very small dipoles the charge density vanishes.

Figure 19 shows the conditional probability density $p(s|x)$ as a function of the projection s of dipoles to the x direction. Two different surface charge densities are given for the dipoles of length $l = 2$ nm. We use nonlinearized modified PB theory. The calculation is made for reference charges located at coordinates $x = 0$, $x = 1$ nm, $x = 5$ nm, and $x = 10$ nm. In the interval $0 < x < 2$ nm the conditional probability densities are defined only in the interval $-x < s < l$, while in the interval 8 nm $< x < 10$ nm the conditional probability densities are defined in the interval $-l < s < D - x$. The conditional probability density increases with increasing s. For $x = 0$, $x = 1$ nm and $x = 5$ nm the conditional probability density reaches its maximum at $s = +l$, while for $x = 10$ nm the conditional probability density reaches its maximum at $s = D - x$.

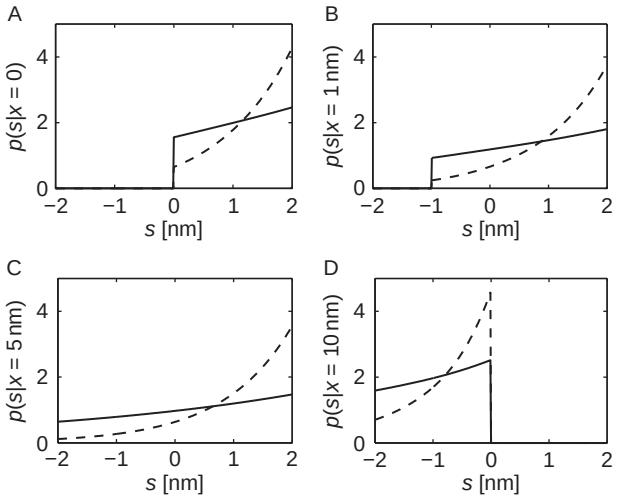

Figure 19 Conditional probability density as a function of the projection of the dipoles with respect to the axis x for four different coordinate of the reference charge (A) $x = 0$, (B) $x = 1$ nm, (C) $x = 5$ nm and (D) $x = 10$ nm [4]. The surface charge densities are $\sigma = 0.005$ As/m^2 (full lines) and $\sigma = 0.02$ As/m^2 (dashed lines). The volume of dipole is $v_0 = l\, a_0$. The nonlinear PB theory is used. The model parameters are $l = 2$ nm, $D = 10$ nm, $a_0 = 1$ nm^2 and $Z = 1$ and $N = 25$ for $A = 100$ nm^2.

6. Concluding Remarks

In this work we present the review on the functional density theory of the electric double layer developed on the basis of statistical mechanical description. The procedure is derived, which starts with the energies of individual particles, obtaining expressions for particle distribution functions and differential equation for the electrostatic potential in different geometries and considering different properties of charged nanoparticles composing the solution. The finite size of charged nanoparticles is considered by the excluded volume effect. We have derived a density functional theory for rod-like ions of arbitrary length. The specific application to the case of two interacting, like-charged, planar charged surfaces reveals the possibility of attractive interactions, introduced solely by correlations within the rod-like ions.

The introduction of the excluded volume effect in the PB theory within the lattice model approach [34] allows for an improved description of the electrostatics of charged membranes, charged cylindrical tubes and spheres filled with electrolyte solution. The model distinguishes between occupied and free lattice sites. Free lattice sites are assumed to be occupied by water with a relative permittivity of 78.5. Consequently, the ions are assumed to be suspended in a continuous dielectric medium.

In PB theory, ions are considered to be dimensionless. Thus, the counter-ion concentration near a charged surface can increase boundlessly. As a result, the results

of the PB theory show a continuous increase in counter-ion concentration near the surface, with increasing $|\sigma|$ (Fig. 8). In contrast to the PB theory, in *excluded volume functional density* (EVFD) theory the ions are assumed to have finite size. This assumption has a considerable effect on counter-ion concentration and the electrostatic potential profiles. The EVFD theory predicts a plateau of counter-ion concentration close to the charged surface [34,35,59,57], a finding supported by recent experimental findings on planar electric double layers [64]. The deviation from the predictions of the PB theory could be attributed to the steric effect (Fig. 8) where the number density of ions cannot exceed the density of the lattice sites.

With decreasing radius, the number of lattice sites declines faster in the spherical than in the cylindrical geometry. Therefore the concentration of counter-ions at the axis of a cylinder reaches a plateau at lower $|\sigma|$ than in the center of a sphere. In cylindrical geometry, counter-ion condensation is observed at lower $|\sigma|$ than in the spherical geometry.

The measure was introduced that describes an effective thickness of the electric double layer, a distance where the density of the number of counter-ions drops to a chosen fraction of its maximal value. It was shown that the effective thickness of the electric double layer increases with increasing counter-ion size.

The functional density theory for rod-like ions of arbitrary length, l, used in the case of two interacting, like-charged, planar surfaces, reveals the possibility of attractive interactions. In our present approach, the critical rod length for the attraction (l_c) is roughly given by twice the Debye length l_D that characterizes the electrostatic screening length (i.e., $l_c \approx 2l_D$). In the limit of large rod length ($l \gg l_D$) an equilibrium distance $D \approx l$ between the charged surfaces results from a bridging interaction. We expect that our present results contribute to better understanding of protein-induced agglutination of like-charged membrane surfaces [7,63] and the nature of condensation of DNA [66,67] and other macroions by the rod-like structured common condensing agents such as polyamines and certain linear peptides.

We also considered a system of two oppositely charged surfaces in a solution composed of dipoles and monovalent ions. The density functional theory for dipoles of arbitrary length was introduced. The spatial distribution of electric charge within the dipoles, the orientations of dipoles and their restrictions near the charged surface were taken into account. The numerical solution showed that the dipoles are predominantly oriented parallel to the electric field, i.e., perpendicular to the charged surfaces. The interaction between oppositely charged surfaces mediated by dipoles was discussed. The presence of the dipoles in the electrolyte solution affects the interaction between two oppositely charged surfaces. The force between the oppositely charged surfaces is especially pronounced at the distance between charged surface being equal to the length of the dipoles, which is related to the bridging mechanism [68].

In summary, we studied the electric double layer in different geometries and compositions. In our theory the finite size of ions and charge distribution within the large quadrupolar (divalent) or dipolar ions was taken into account. The described physical properties of the electric double layer may in the future attract increasing attention owing to their benefit in technology, biology and medicine.

REFERENCES

[1] J.N. Israelachvili, Intermolecular and Surface Force Academic Press, London/San Diego, 1992.
[2] A. Safran, Statistical Thermodynamics of Surfaces, Interfaces, and Membranes Addison-Wesley, Colorado, 1994.
[3] K. Bohinc, A. Iglič, S. May, Interaction between macroions mediated by divalent rod-like ions, Europhys. Lett. 68 (2004) 494–500.
[4] S. Maset, K. Bohinc, Orientations of dipoles restricted by two oppositely charged walls, J. Phys. A: Math. theor. 40 (2007) 11815–11826.
[5] S. Sylvio May, A. Iglič, J. Reščič, S. Maset, K. Bohinc, Bridging like-charged macroions through long divalent rod-like ions, J. Phys. Chem. B 112 (2008) 1685–1692.
[6] O. Alvarez, M. Brodwick, R. Latorre, A. Mclaughlin, S. Mclaughlin, G. Szabo, Large divalent cations and electrostatic potentials adjacent to membranes, Biophys J. 44 (1983) 333–342.
[7] J. Urbanija, N. Tomšič, M. Lokar, A. Ambrožič, S. Čučnik, B. Rozman, M. Kandušer, A. Iglič, V. Kralj-Iglič, Coalescence of phospholipid membranes as a possible origin of anticoagulant effect of serum proteins, Chem. Phys. Lipids 150 (2007) 49–57.
[8] S. McLaughlin, The Electrostatic properties of membranes, Ann. Rev. Biophys. Chem. 18 (1989) 113–136.
[9] R. Heinrich, M. Gaestel, R. Glaser, The electric potential profile across the erythrocyte membrane, J. Theor. Biol. 96 (1982) 211–231.
[10] A. Iglič, M. Brumen, S. Svetina, Determination of the inner surface potential of the erythrocyte membrane, Bioelectrochemistry 43 (1997) 97–103.
[11] A. Karlsson, R. Karlsson, M. Karlsson, A.S. Cans, A. Strömberg, F. Ryttsen, O. Orwar, Networks of nanotubes and containers, Nature 409 (2001) 150–152.
[12] V. Kralj-Iglič, A. Iglič, G. Gomišček, V. Arrigler, H. Hägerstrand, Microtubes and nanotubules of phospholipid bilayer vesicles, J. Phys. A: Math. Gen. 35 (2002) 1533–1549.
[13] A. Iglič, H. Hägerstrand, V. Arrigler, V. Kralj-Iglič, Possible role of phospholipid nanotubules in directed transport of membrane vesicles, Phys. Lett. 310 (2003) 493–497.
[14] A. Rustom, R. Saffrich, I. Markovič, P. Walther, H.H. Gerdes, Nanotubular highways for intercellular organelle transport, Science 303 (2004) 1007–1010.
[15] A. Iglič, M. Lokar, B. Babnik, T. Slivnik, P. Veranič, H. Hägerstrand, V. Kralj-Iglič, Possible role of flexible red blood cell membrane nanodomains in the growth and stability of membrane nanotubes, Blood Cells Mol. Dis. 39 (2007) 14–23.
[16] K. Bohinc, T. Slivnik, A. Iglič, M. Brumen, V. Kralj-Iglič, Transmembrane distribution of membrane constituents in organic nanotubes driven by electric charge and intrinsic anisotropy of molecules, J. Phys. Chem. C 111 (2007) 9709–9718.
[17] N. Imai, T. Ohinshi, Analytical solution of Poisson–Boltzmann equation for two-dimensional many-center problem, J. Chem. Phys. 30 (1959) 1115–1116.
[18] F. Oosawa, Polyelectrolytes Marcel Dekker, New York, 1970.
[19] G.S. Manning, Limiting Laws and Counterion Condensation in Polyelectrolyte Solutions I Colligative Properties, J. Chem. Pys. 51 (1969) 924–933.
[20] K.S. Schmitz, Macroions in Solution and Colloidal Suspension, VCH Publishers, New York, 1993.
[21] M.G. Gouy, Sur la constitution de la charge electrique ala surface d'un electrolyte, J. Phys. Radium (Paris) 9 (1910) 457–468.
[22] D.L. Chapman, A Contribution to the Theory of Electrocapillarity, Philos. Mag. 6 (1913) 475–481.
[23] S.L. Carnie, D.Y.C. Chan, J. Stankovich, Computation of forces between spherical colloidal particles-nonlinear Poisson–Boltzmann theory, J. Coll. Interface Sci. 165 (1994) 116–128.
[24] D. Bratko, V. Vlachy, Distribution of counterions in the double layer around a cylindrical polyion, J. Phys. Chem. 90 (1982) 434–438.
[25] T. Das, D. Bratko, L.B. Bhuiyan, C.W. Outhwaite, Modified Poisson–Boltzmann Theory Applied to Linear Polyelectrolyte Solutions, J. Phys. Chem. 99 (1995) 410–418.

[26] T. Das, D. Bratko, L.B. Bhuiyan, C.W. Outhwaite, Polyelectrolyte solutions containing mixed valency ions in the cell model: A simulation and modified Poisson–Boltzmann theory, J. Phys. Chem. 107 (1997) 9197–9207.
[27] E. Gonzalez-Tovar, M. Lozada-Cassou, D. Henderson, Hypernetted chain approximation for the distribution of ions around a cylindrical electrode. II. Numerical solution for a model cylindrical polyelectrolyte, J. Chem. Phys. 83 (1985) 361–372.
[28] G.M. Torrie, J.P. Valleau, Electrical double-layers 4 Limitations of the Gouy–Chapman theory, J. Phys. Chem. 86 (1982) 3251–3257.
[29] M. Lozado-Cassou, D. Henderson, Application of the hypernetted chain approximation to the electrical double layer Comparison with Monte Carlo results for 2:1 and 1:2 salts, J. Phys. Chem. 87 (1983) 2821–2824.
[30] R. Bacquet, P.J. Rossky, Corrections to the HNC equation for associating electrolytes, J. Chem. Phys. 79 (1983) 1419–1426.
[31] R. Bacquet, P.J. Rossky, Ionic Atmosphere of Rodlike Polyelectrolytes. A Hypernetted Chain Study, J. Phys. Chem. 88 (1984) 2660–2669.
[32] V. Freise, Zur Theorie der Diffusendoppeltschicht, Z. Elektrochem. 56 (1952) 822–827.
[33] M. Eigen, E. Wicke, The Thermodynamics of Electrolytes at Higher Concentrations, J. Phys. Chem. 58 (1954) 702–714.
[34] V. Kralj-Iglič, A Simple Statistical Mechanical Approach to the Free Energy of the Electric Double Layer Including the Excluded Volume Effect, J. Phys II France 6 (1996) 477–491.
[35] I. Borukhov, D. Andelman, H. Orland, Steric Effects in Electrolytes: A Modified Poisson Boltzmann Equation, Phys. Rev. Lett. 79 (1997) 435–438.
[36] M. Manciu, E. Ruckenstein, Lattice Site Exclusion Effect on the Double Layer Interaction, Lamgmuir 18 (2002) 5178–5185.
[37] I. Borukhov, Charge renormalization of cylinders and spheres: Ion size effect, J. Pol. Sci. B: Pol. Phys 42 (2004) 3598.
[38] E. Trizac, J.L. Raimbault, Long-range electrostatic interactions between like-charged colloids: Steric and confinement effects, Phys. Rev. E 60 (1999) 6530–6533.
[39] G. Barbero, L.R. Evangelista, D. Olivero, Asymmetric ionic adsorption and cell polarization in liquid crystals, J. Appl. Phys. 87 (2000) 2646–2648.
[40] L. Lue, N. Zoeller, D. Blankschtein, Incorporation of Nonelectrostatic Interactions in the Poisson–Boltzmann Equation, Langmuir 15 (1999) 3726–3730.
[41] S. Lamperski, C.W. Outhwaite, Exclusion volume term in the inhomogeneous Poisson–Boltzmann theory for high surface charge, Langmuir 18 (2002) 3423–3424.
[42] P. Mills, C.F. Anderson, M.T. Record, Monte Carlo studies of counterion-DNA interactions. Comparison of the radial distribution of counterions with predictions of other polyelectrolytes theories, J. Phys. Chem. 89 (1985) 3984–3994.
[43] L.B. Bhuiyan, C.W. Outhwaite, D. Bratko, Structure and thermodynamics of micellar solutions in the modified Poisson–Boltzmann theory, Chem. Phys. Lett. 193 (1992) 203–210.
[44] D. Bratko, Hypernetted chain approximation for ion distribution in reverse micelles, Chem. Phys. Lett. 169 (1990) 555–560.
[45] W.M. Gelbart, R. Bruinsma, P.A. Pincus, V.A. Parsegian, DNA-Inspired Electrostatics. Not just the repository of our genetic information, DNA is also a fascinating, shape-shifting molecule whose behavior in solution counters our intuition and challenges our physical understanding, Phys. Today 53 (2000) 38–44.
[46] V.A. Bloomfield, DNA condensation, Curr. Opin. Struct. Biol. 6 (1996) 334–341.
[47] T.E. Angelini, H. Liang, W. Wriggers, G.C.L. Wong, Like-charge attraction between polyelectrolytes induced by counterion charge density waves, Proc. Natl. Acad. Sci. USA 100(15), (2003) 8634–8637.
[48] J.C. Butler, T. Angelini, J.X. Tang, G.C.L. Wong, Ion multivalence and like-charge polyelectrolyte attraction, Phys. Rev. Lett. 91(2), (2003) 028301/1–4.
[49] A.Y. Grosberg, T.T. Nguyen, B.I. Shklovskii, The physics of charge inversion in chemical and biological systems, Mod. Rev. Phys. 74 (2002) 329–345.
[50] R.R. Netz, Electrostatistics of counter-ions at and between planar charged walls: From Poisson–Boltzmann to the strong-coupling theory, Eur Phys. J. E 5 (2001) 557–574.

[51] P. Linse, Mean force between like-charged macroions at high electrostatic coupling, J. Phys.: Condens. Matter 14 (2002) 13449–13467.
[52] L. Guldbrand, B. Jönsson, H. Wennerström, P. Linse, Electrical double layer forces. A Monte-Carlo study, J. Chem. Phys. 80(5), (1984) 2221–2228.
[53] R. Kjellander, S. Marčelja, Surface interactions in simple electrolytes, J. Phys. France 49(6) (1988) 1009–1015.
[54] R. Kjellander, Ion–ion correlations and effective charges in electrolyte and macroion systems, Ber. Bunsenges. Phys. Chem. 100(6), (1996) 894–904.
[55] J.D. Jackson, Classical Electrodynamics Wiley, New York, 1999.
[56] T.L. Hill, An Introduction to Statistical Thermodynamics, Adison-Wesley, Reading, MA/ Toronto, Canada, 1962.
[57] K. Bohinc, J. Gimsa, V. Kralj-Iglič, T. Slivnik, A. Iglič, Excluded volume driven counterion condensation inside nanotubes in a concave electrical double layer model, Bioelectrochemistry 67 (2005) 91–99.
[58] L.E. Elsgolc, Calculus of Variations, Pergamon Press, Oxford, UK, 1961.
[59] K. Bohinc, V. Kralj-Iglič, A. Iglič, Thickness of electrical double layer Effect of ion size, Electrochim. Acta 46 (2001) 3033–3040.
[60] K. Bohinc, A. Iglič, T. Slivnik, V. Kralj-Iglič, Planar, cylindrical and spherical electrical doule layers in biological systems. The effect of counterions, Cell. Mol. Biol. Lett. 7 (2002) 839–843.
[61] D.F. Evans, H. Wennerström, The colloidal domain, where physics, chemistry, and biology meet (2nd ed.), VCH, New York, 1994.
[62] D. Andelman, Handbook of Biological Physics, Vol. 1. Elsevier, Amsterdam, 1995.
[63] J. Urbanija, V. Kralj-Iglic, A. Bellen, S. Maset, P.B.S. Kumar, A. Iglic, K. Bohinc, Attraction between negatively charged surfaces mediated by extended charges, submittedfor publication.
[64] N. Cuvillier, F. Rondelez, Breakdown of the Poisson–Boltzmann description for electrical double layers involving large multivalent ions, Thin Solid Films 327–329 (1998) 19–23.
[65] A. Abrashkin, D. Andelman, H. Orland, Dipolar Poisson–Boltzmann Equation: Ions and Dipoles Close to Charge Interfaces, Phys. Rev. Lett. 99(2007) 077801/1-4.
[66] V.A. Bloomfield, DNA condensation by multivalent cations, Biopolymers 44 (1997) 269–282.
[67] V.B. Teif, Ligand-induced DNA condensation: Choosing the model, Biophys. J. 89 (2005) 2574–2587.
[68] E.E. Meyer, Q. Lin, T. Hassenkam, E. Oroudjev, J.N. Israelachvili, Origin of the long-range attraction between surfactant-coated surfaces, Proc. Natl. Acad. Sci. USA 102 (2005) 6839–6842.